Universidade de Aveiro Departamento de Engenharia de Materiais e Cerâmica
2014

Manuela Alexandra Coelho Fernandes

Estudos de fronteira de grão em titanatos

Studies of grain boundaries in titanates

Universidade de Aveiro
2014
Departamento de Engenharia de Materiais e Cerâmica

Manuela Alexandra Coelho Fernandes

Estudos de fronteira de grão em titanatos

Dissertação apresentada à Universidade de Aveiro para cumprimento dos requisitos necessários à obtenção do grau de Mestre em Engenharia de Materiais, realizada sob a orientação científica da Doutora Ana Maria de Oliveira e Rocha Senos, Professora Associada do Departamento de Engenharia de Materiais e Cerâmica da Universidade de Aveiro e da Doutora Paula Maria Lousada Silveirinha Vilarinho, Professora Associada do Departamento de Engenharia de Materiais e Cerâmica da Universidade de Aveiro.

O jurí

presidente

Prof. Doutor Jorge Ribeiro Frade
Professor catedrático da Universidade de Aveiro

Prof. Doutor João Carlos de Castro Abrantes
Professor adjunto da Escola Superior de Tecnologia e Gestão – Instituto Politécnico de Viana do Castelo

Prof. Doutora Ana Maria de Oliveira e Rocha Senos
Professora associada da Universidade de Aveiro

Acknowledgements

I would like to express my deepest gratitude to my supervisors, Prof. Dr. Ana Senos and Prof. Dr. Paula Vilarinho, for their guidance, support.suggestions, discussions and patience. Many thanks to Nivas for his help during this work, in special with the electrical measurements.

I would like to thanks to all the technicians of the department of materials and ceramics engineering for their generous help. I am also grateful to Electroceramics groups for a great work environment.

A lot of thanks to my friends, in special to Cátia Ferreira for her precious friendship, her continuous support and for making my days brighter; and to João Resende for his “lack of patience” and his friendship. To both of you, thanks for being there every time that I need.

I am very grateful to my better half, Ivo Angélico, for his love, his patience, his support and for his continuous understanding.

Finally, I would like to thanks to my mother for her support, to my sister and to my brother.

palavras-chave

Microestrutura, fronteiras de grão, $BaLa_4Ti_4O_{15}$, atmosfera de sinterização, crescimento de grão, propriedades dieléctricas

resumo

Dispositivos microelectrónicos para sistemas de comunicação têm-se tornado cada vez mais pequenos e, como consequência, são necessários materiais com melhores propriedades. Os dieléctricos devem apresentar valores elevados para a permitividade relativa, baixas perdas dieléctricas e um coeficiente de temperatura à frequência de ressonância próximo de zero para ser possível reduzir o tamanho dos equipamentos.

A maior dificuldade está em encontrar um material com valores óptimos para todos os requisitos em simultâneo e o BLT é um titanato com elevada permitividade relativa, um coeficiente de temperatura à frequência de ressonância próximo de zero e baixas perdas dieléctricas. A atmosfera de sinterização influencia as características das fronteiras de grão e, consequentemente, o tamanho de grão e a razão de aspecto. Contudo, não existem estudos sobre a influência desta variável nas características do BLT.

Neste estudo foi preparado pó de BLT e conformadas amostras volúmicas por prensagem. Os compactos de BLT foram sinterizados em atmosferas de azoto, oxigénio e em ar durante tempos variáveis entre 0 e 10 horas. Foi realizada uma caracterização microestrutural e foram medidos parâmetros como o tamanho de grão e a razão de aspecto dos grãos. As amostras sinterizadas em oxigénio apresentaram uma densidade elevada e um tamanho de grão maior do que as amostras sinterizadas em azoto. A razão de aspecto aumenta com o aumento do tempo de sinterização para ambas as atmosferas, mas mostrou-se mais elevada no caso do oxigénio.

Foi detectada uma segunda fase em amostras sinterizadas em oxigénio e azoto. Nas amostras sinterizadas em oxigénio está presente titanato de lantânio e nas amostras sinterizadas em azoto está presente titanato de bário, devido à química de defeitos deste material.

Foram também medidas a permitividade relativa, as perdas dieléctricas, a condutividade e o coeficiente de temperatura da permitividade relativa. Amostras sinterizadas durante 0 horas em azoto mostraram os valores mais elevados de permitividade relativa e de condutividade. O coeficiente de temperatura da permitividade relativa foi calculado a 1 MHz e obtiveram-se valores próximos de zero para ciclos de sinterização com mais de 30 minutos de patamar a 1530 ºC.

keywords

Microstructures, grain boundaries, $BaLa_4Ti_4O_{15}$, sintering atmosphere, grain growth, dielectric properties.

abstract

Microelectronic devices for communication systems are becoming smaller and, as consequence, materials with better properties are needed. Dielectric ceramics with a high relative permittivity, low dielectric losses and a near-zero temperature coefficient of resonant frequency are the materials requisites for device miniaturization.

The greatest difficult is to find a material with optimal values for all requisites and BLT is a titanate with a higher relative permittivity, a near-zero temperature coefficient of resonant frequency and low losses. The sintering atmosphere has influence in the grain boundary characteristics and consequently in the grain size and grain aspect ratio. However, there are no studies of the influence of the sintering atmosphere in the BLT characteristics.

In this study, the BLT powder was prepared and bulk ceramics were pressed. Compacts were sintered under nitrogen, oxygen and air between 0 and 10h. Microstructure characterization was performed and the grain size and grains aspect ratio were measured. A higher density and a higher grain size were achieved for samples sintered in oxygen. The aspect ratio increases with the increasing of sintering time for both atmospheres, but is higher for oxygen.

A second phase was found in samples sintered in oxygen and nitrogen. A lanthanum titanate is present in samples sintered in oxygen and a barium titanate is present in samples sintered in nitrogen due to the defect chemistry.

Relative permittivity, dielectric losses, conductivity and temperature coefficient of relative permittivity were measured. A higher relative permittivity, as the higher conductivity, was achieved in the sample sintered in nitrogen for 0 hours. A temperature coefficient of relative permittivity was calculated at 1 MHz and values around zero were obtained for sintering cycles with more than 30 minutes of dwell time at 1530 ºC.

Table of contents

List of Figures

List of Tables

List of symbols

a, c – lattice parameters

c – speed of the light in a vacuum media

d – density

D – diameter

D_a - diffusion coefficient for atomic motion across the grain boundary

d_{air} – air density

$D_b^{\perp}$ - atom diffusion coefficient across grain boundary

D_g – geodesic diameter

d_{liq} – liquid density

F_b - driving force for grain boundary migration

F_d – drag force of a particle against the boundary movement

F_g – shape factor

f_r – resonant frequency

G – grain size

I – current

k – Boltzmann constant

m – mass

M_b – grain boundary mobility

pO_2 – oxygen partial pressure

Q – quality factor

R – gas constant

R – resistance

S – particle area

t – sintering time

T – temperature

Ts - Start shrinkage temperature

T_{max} - temperature for the maximum velocity

t_f - temperature coefficient of resonant frequency

tan δ – dielectric losses

$TC\varepsilon_r$ - temperature coefficient of relative permittivity

U – voltage

V – volume

v_b – grain boundary velocity

V_m – molar volume

V_{max} - maximum velocity

W_1, W_2 – sample weigth in air and liquid, respectively

Z' – real part of impedance

Z'' – complex part of impedance

α – thermal expansion

β – proportional constant

γ_{gb} - grain boundary energy

δ_{gb} – grain boundary width

ε_{eff} - effective permittivity

ε_{gb} - dielectric constant of the grain boundary

ε_r – relative permittivity

ε – absolute permittivity

ε_0 – permittivity of free space

θ – phase angle

λ_0 – vacuum wavelength at resonance frequency

λ_d – wavelength of the standing wave along the diameter of the resonator

τ_f – temperature coefficient of resonant frequency

ω – angular frequency

Ω – atomic volume

List of abbreviations

AC – Alternating current

BLT – barium lanthanum titanate ($BaLa_4Ti_4O_{15}$)

BNT - Barium Neodimium Titanate ($Ba_{4.5}Nd_9Ti_{18}O_{54}$)

ccp – cubic close-packed

CCTO - $CaCu_3Ti_4O_{12}$

CIP – Cold Isostatic Pressing

DC – Direct current

EDAX - energy dispersive analysis of X-rays

EDS – Energy Dispersive Spectroscopy

GPS – global positioning system

hcp – hexagonal close-packed

HIP – Hot Isostatic Pressing

HP – Hot Pressing

IS – Impedance Spectroscopy

SEM – Scanning Electron Microscope

TEM – Transmission Electron Microscope

XRD – X-Ray Diffraction

Chapter 1

Introduction

1.1Motivation

The electric properties of polycrystalline materials are markedly affected by grain boundaries and their characteristics[4], that instead are influenced by some processing variables, such as sintering temperature, sintering atmosphere and applied pressure.

Among these variables, the sintering atmosphere is one of the most studied and the literature is rich in examples of relations between sintering atmosphere, defect chemistry, microstructure development and electrical properties. A typical case is the one of $BaTiO_3$ in which the semiconductor behavior found application as PTC (positive temperature coefficient) thermistors. However in what concerns the families of rare earth titanates (tungsten bronze $BaTiO_3$–Ln_2O_3–TiO_2 (Ln - Lathanide, i.e. Nd, Sm, La etc), for high frequency applications, these studies are rare and not reported for BLT.

A study in sintering of BLT thick films was performed in our investigation group. Stresses between the substrate and the film caused an anisotropic grain growth with elongated grains and preferentially oriented in a parallel way to the substrate. In addition, it was observed a difference in grain size between these films and a BLT bulk ceramic sintered without applied pressure, being smaller in the bulk ceramic than in the films [2]. The dielectric response, particularly of $TC\varepsilon_r$, of these films is dependent on the microstructure anisotropy degree.

A grain growth anomaly in strontium titanate ($SrTiO_3$) was reported by this group.[5] A discontinuous grain growth with the sintering temperature was observed and four grain growth regimens, with a grain size drop, were identified. These transitions occurred at 1500, 1550 and 1605 ºC. The same trend was found for the grain boundary thickness and grain boundary activation energy, affecting the strontium titanate dielectric properties. This anomaly suggests the presence of different grain boundary phases (complexions).

Another study in sintering of strontium titanate was done and it' showed a high-temperature resistance anomaly related with the faceting and defaceting of grain boundaries. Below 1600˚C an electric response was seen which corresponds to the bulk and above this temperature we identified an electric response corresponding to the grain boundaries. This could be related to the faceting and defaceting of the grain boundaries, since this transition occurs at 1600 ˚C[6].

The sintering atmosphere is other variable that affects the grain boundary characteristics and the electrical properties of the material. A study performed in niobium-doped $SrTiO_3$ shows distinct solute segregation in samples sintered at a reducing atmosphere (H_2) and in air, which cause a differentiated electrical behavior [7].

Microelectronic devices for communication systems are becoming smaller and required to work at higher frequencies; as a consequence, materials with higher dielectric permittivity ($20<\varepsilon_r<100$) are required. Low dielectric losses and good temperature stability of the dielectric response are needed. Among others, $BaLa_4Ti_4O_{15}$ (hereafter designated by BLT) is one titanate of the tungsten bronze $BaTiO_3$-Ln_2O_3-TiO_2 (Ln – lanthanide) with the desired properties for these applications[2].

In resume, the results of our group and others in the open bibliography show that the sintering variables can be used to design the microstructure of titanate materials, changing the grain boundary characteristics and the electrical response of the material. However, the understanding of the effect of the sintering variables at the grain boundary level is yet embrionary and more research on this topic is clearly missing, namely in functional ceramics. Among others, $BaLa_4Ti_4O_{15}$ (hereafter designated by BLT) is one titanate of the tungsten bronze $BaTiO_3$-Ln_2O_3-TiO_2 (Ln – lanthanide) with very interesting properties for microelectronic devices in communication systems and no studies in terms of the effect of the sintering atmosphere on the microstructural design and electrical properties were reported.

1.2 Objectives of this thesis

Within this context, the objective of this work is to study the influence of the sintering atmosphere on the grain boundaries composition and electrical properties of $BaLa_4Ti_4O_{15}$.

Chapter 2

State of the art

This chapter presents some important electrical properties of microwave ceramics, such as relative permittivity, dielectric losses and temperature coefficient of resonance frequency. Some aspects of BLT crystal structure and some defect chemistry of La-doped $BaTiO_3$ are mentioned. An overview of the effect of the sintering temperature, the sintering atmosphere and the pressure in titanates is presented.

2.1 Electrical properties of microwave ceramics

Microelectronics technology has very much influencing in our day to day life, one of its main attraction is the miniaturization and can be seen in cellular phones with a constant decrease in size and weight. Communication systems are an example of microelectronics devices, which works at microwave frequencies (0.3 – 100 GHz)[8]. At the lowest frequencies works radar for military applications, Ultra High Frequency Broadcast TV and cellular phones, whereas the satellite communication and GPS systems operate at higher frequencies[9].

Dielectric ceramics, such as titanates, play an important role in the microwave wireless communication due to the possibility of reduced size and low cost of some components of these devices (resonators and filters), allowing the continuous miniaturization. It is well understood that the evolution of wireless communication technology could only happen due to advances in materials[10]. The crystal structure and several parameters, such as purity of starting materials, conformation method and sintering temperature and duration are important to achieve the desired properties for microwave applications[9,10].

2.1.1 Relative permittivity

A material is classified as “dielectric” if it has the ability to store energy when an external electric field is applied. When a DC source is placed across a parallel plate capacitor more charge can be stored if we fill the dielectric material between plates

replacing the vacuum. This increase in storage capacity is due to the neutralization of charge carriers by the dielectric materials, otherwise these charge carriers will contribute to the external field. If we are applying an AC sinusoidal voltage, the resulting currents will have two components namely charging current and loss current which is related to the dielectric constant of the material. And in this case the dielectric constant will be a complex number, the complex dielectric constant will have a real part which represents the storage and imaginary part which represents the loss. Dielectric constant is equitant to the relative permittivity (ε_r) or the ratio between absolute permittivity (ε) and the permittivity of free space (ε_0). The real part of relative permittivity ($\varepsilon_{r'}$) is a measure of amount of energy stored from the external field while the imaginary part ($\varepsilon_{r''}$) is related with the amount of energy loss, which indicates how dissipative is the material for an external field. This imaginary part of relative permittivity includes both dielectric loss and conductivity.

Materials for microwave applications must have three prerequisites. The most important for device miniaturization is a high relative permittivity ($\varepsilon_r > 25$)[11,12] which allows to reduce the size of resonators, because size is inversely proportional to the square root of relative permittivity[10,11,13]:

$$\mathbf{D} = \boldsymbol{\lambda_0} \frac{\mathbf{1}}{\sqrt{\boldsymbol{\varepsilon_r}}} \tag{2-1}$$

where D is the diameter of the resonator and λ_0 is the vacuum wavelength at resonance frequency. If the permittivity is increased the size may be decreased[11].

The relative permittivity is also related with the resonant frequency (f_r) of the dielectric resonator:

$$\boldsymbol{f_r} = \frac{\boldsymbol{c}}{\boldsymbol{\lambda_d}\sqrt{\boldsymbol{\varepsilon_r}}} \approx \frac{\boldsymbol{c}}{\boldsymbol{D}\sqrt{\boldsymbol{\varepsilon_r}}} \tag{2-2}$$

where c is the speed of the light in a vacuum and λ_d is the wavelength of the standing wave along the diameter of the resonator[11,14].

2.1.2 Dielectric Losses

Other important requirement is low dielectric losses (tan δ) or a high quality factor Q (> 5000 between 5-10GHz) to optimize the signal intensity. The quality factor, Q, is defined by[12,15]:

$$\boldsymbol{Q = \frac{1}{\tan \delta}} \tag{2-3}$$

Microwave engineers utilized the product of the quality factor by the resonant frequency, Q x f_r, to characterized the microwave dielectric. This product should be constant and usually is used to compare materials[11,14].

2.1.3 Temperature coefficient of resonance frequency

The third requisite is a near zero temperature coefficient of resonant frequency (t_f = 0 ± 5 ppm/°C). This parameter (t_f) characterizes the thermal stability of the material and is related to the temperature coefficient of relative permittivity (TCε_r) and the coefficient of thermal expansion (α) by the expression[14]:

$$\boldsymbol{t_f = -\left(\frac{TC\varepsilon_r}{2} - \alpha\right)} \tag{2-4}$$

TCε_r is obtained measuring the relative permittivity at different temperatures and calculated using the following equation[16]:

$$\boldsymbol{TC\varepsilon_r = \frac{\Delta \varepsilon_r}{\varepsilon_{r0} \Delta T}} \tag{2-5}$$

Temperature coefficient of relative permittivity depends on many factors, including tolerance factor[17] and aspect ratio[18]. Zhi Fhu *et al* reported an increasing of the TCε_r with the increasing of the aspect ratio in BNT thick films (Figure 1).

Some materials with good properties for microwave applications were referred by Wersing and the table 1 contains the values of relative permittivity, temperature coefficient of the resonant frequency and quality factor Q for these materials.

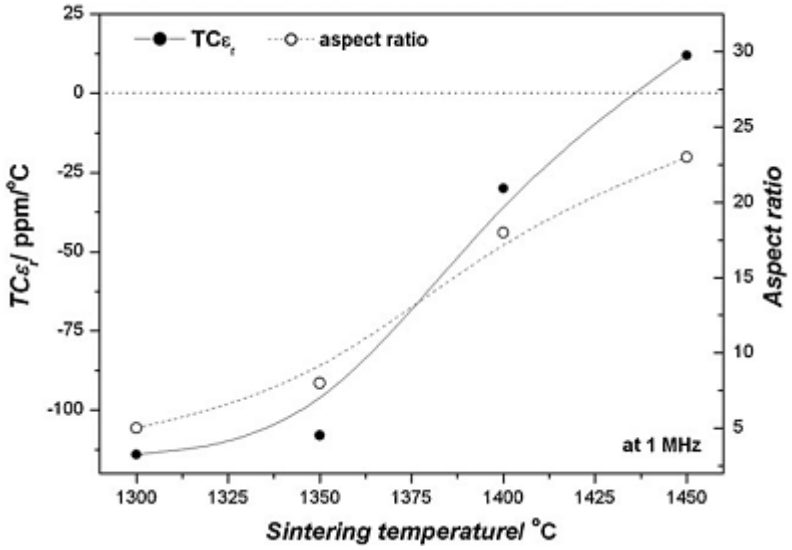

Figure 1 - Dependence of $TC\varepsilon_r$ and aspect ratio of BNT thick films on the sintering temperature [18].

As it is possible to see in table 1, it is difficult to find materials with optimal values for these requirements simultaneously, there exists materials with excellent quality factor, a temperature coefficient of the resonant frequency approximately zero, nonetheless, a relative permittivity lower than some other materials.

Before 1996 there are no reports of dielectric properties of $BaLa_4Ti_4O_{15}$, but Vineis et al has made the first measurements the properties in BLT and has reported a Q x f_r of 11583 GHz, a temperature coefficient of the resonant frequency (t_f) of -17 ppm/˚C and a relative permittivity (ε_r) of 43[12]. In 2006 Zheng et al has reported a higher quality factor Q than Vineis et al (44000 at 4 GHz), a ε_r of 45 and a t_f of -2ppm/˚C[19]. As we can see $BaLa_4Ti_4O_{15}$ fills the requisites to be used in the applications cited above.

Table 1 - Important groups of microwave ceramics[3].

Ceramic	ε_r	t_f (ppm/K)	Q		Ref.
			At 2 GHz	At 20 GHz	
$Ba_2Ti_9O_{20}$	40	2	15000	2000	[3]
$Zr_{0.8}TiSn_{0.2}O_4$	38	0	15000	3000	[3]
$BaTi_u[(Ni_xZn_{1-x})_{1/3}Ta_{2/3}]_{1-u}\ O_3$	30	-3 to +3	26000	5000	[3]
$Ba[Sn_x(Mg_{1/3}Ta_{2/3})_{1-x}]O_3$	25	~0	>40000	10000	[3]
Nd_2O_3-BaO-TiO_2-Bi_2O_3	~90	~0	3000	----	[3]
$BiNbO_4$	~40	~30	4000	----	[3]
$Ba_nLa_4Ti_{3+n}O_{12+3n}$ (n=0.8-2)	45	-21 to -12	Q.f= 30000 to 48000		[20]
$Ba_nLa_4Ti_{3+n}O_{12+3n}$ (n=1)	43 to 49	-17 to -2	Q.f= 11583 to 43589		[12,19,21]
$BaNd_2Ti_5O_{14}$	91	-8 to 46	Q = 1771		[16]

2.2 Crystal structure of $BaLa_4Ti_4O_{15}$

$BaLa_4Ti_4O_{15}$, as the majority of the microwave dielectric ceramics, has a perovskite related structure, with the general formula $A_nB_{n-1}\ O_{3n}$ ($n \geq 3$) structure (B-cation deficient perovskite) with A=(Ba, La) and n=5. This structure corresponds to a close-packing of AO3 mixed layers, where A atoms are surrounded by six oxygen atoms and each oxygen atoms has two A atoms linearly coordinated to it among its six nearest neighbors[13,15,19].

To avoid any direct A–A connection, successive layers are shifted from each other, as shown in Figure 2 (b). One quarter of the octahedral interstices between two such layers are surrounded exclusively by oxygen atoms and are occupied by Ti atoms, the small circles in Figure 2 (b) - (d)[19].

The lattice parameters of the hexagonal BLT cell are a = 5.5671 Å and c = 22,4602 Å. This large difference between the lattice parameters promotes the growth of plate-like grains. Grain orientation was reported for others compounds with plate-like grains, such as $SrBi_4Ti_4O_{15}$ [13,15,19].

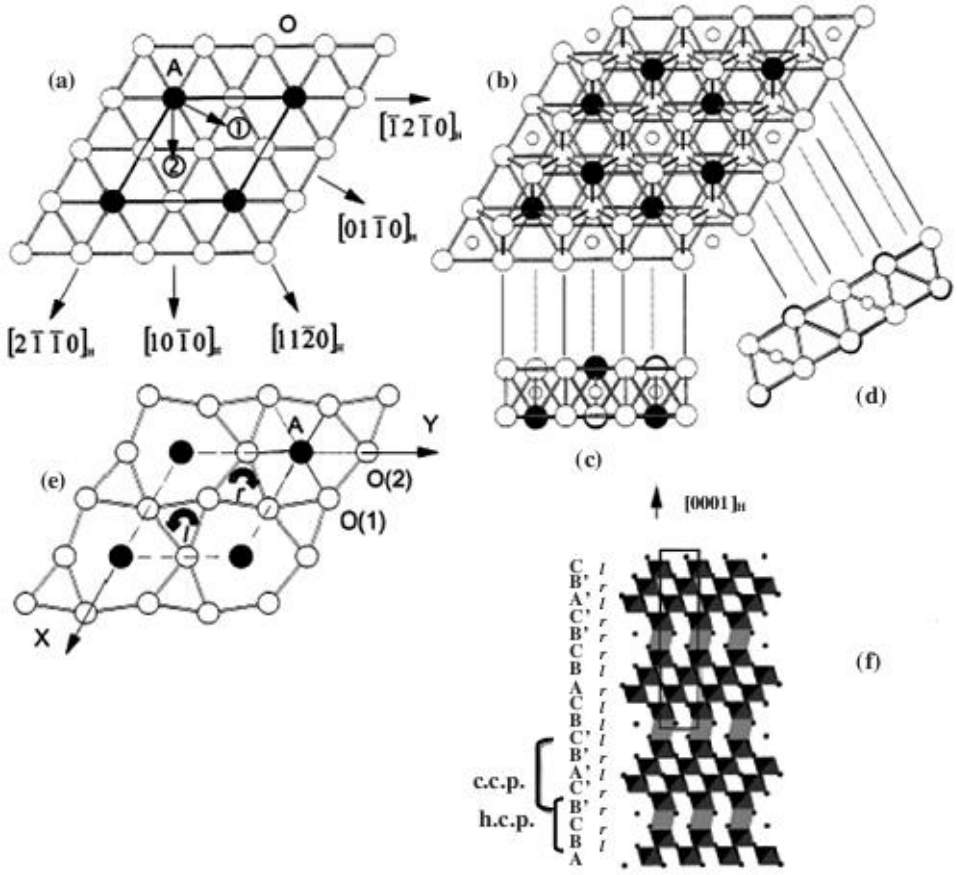

Figure 2 - Schematic views of the AO_3 mixed layers packing in BLT: (a) arrangement of A and O atoms in the AO_3 mixed layers; (b) stacking of two adjacent AO_3 layers, showing the TiO_6 octahedra; (c) view of this stacking along $[10\bar{1}0]_H$; (d) view of this stacking along the $[11\bar{2}0]_H$ direction; (e) the distorted AO_3 layers in BLT–r and l visualize the clockwise and counterclockwise rotations of corner-sharing octahedral respectively; (f) schematic representation of BLT as viewed along $[2\bar{1}\bar{1}0]_H$, where the rotations of TiO_6 octahedra around the c-axis are represented by r (clockwise) and l (counterclockwise). ccp and hcp represent cubic close-packed and hexagonal close-packed, respectively [19].

2.2.1 Defects

Ceramic materials show structural imperfections at temperatures above 0K, which means that perfect crystals do not exist, it is an idealization. The existence of defects in the crystal lattice affects significantly some materials properties.

Defects can be classified by their dimension. Defects classified as 0-dimensional or point-defects involve a single atom or a lattice site in the crystal structure. The 1-dimensional defects are called by dislocations and are a line where the crystal pattern is broken. Defects classified as 2-dimensional defects are surface defects and the 3-dimensional defects are a volume defects, such as precipitates or second-phases.

2.2.1.1 Point defects

This type of imperfections can be intrinsic or extrinsic. There are two types of intrinsic defects: vacancies, when an atom is missing in the crystal structure and interstitialcy, when an atom occupies an interstitial site in the crystal structure. Extrinsic defects are foreign atoms, that can be intentionally added (solutes) or not (impurities), that can occupy a lattice site (substitutional solutes/impurities) or an interstitial site (interstitial solutes/impurities).

The existence of an intrinsic defect changes the charge balance locally, creating an excess charge. This excess charge can be compensated by the existence of a vacancy of other specie nearby. This paired vacancy, formed by an anion and a cation vacancy, is called by Shottky defect. The charge excess created by the existence of a vacancy, on the other hand, can be compensated by adding an interstitial atom of the same specie. This is called Frenkel defect.

The interstitial sites are relatively small and consequently just small atoms, such as hydrogen, carbon and nitrogen, are found as interstitialcy. Larger atoms are usually found as substitutional[22].

Sometimes, point defects are intentionally introduced to semiconductors in order to control the concentration of charge carriers, changing the electrical properties.

2.2.1.2 Other defects

Line defects, also called as dislocations, are 1-dimensional defects and are characterized by a line where occurs a discontinuity in the crystal pattern. There are two main dislocations: edge and screw dislocations. Edge dislocations are easily visualized as

an extra half-plane in the crystal lattice. The atomic bonds are distorted with the movement of this extra half-plane. Screw dislocations are a result of the shear stress and the movement of the defect line is perpendicular to the direction of the stress. Real materials present a mix of these two types of dislocations instead of pure edge or screw dislocations.

Grain boundaries and stacking faults are 2-dimensional defects. Grain boundaries are present in polycrystalline materials due to the different orientation of the grains. A defect in the sequence of atomic planes is called by stacking faults.

Another type of defects that can be present in crystal structures are the 3-dimensional defects or volume defects. This type of defects could be precipitates, inclusions and voids. Precipitates are small particles introduced into the matrix with a defined purpose. Inclusions are larger than precipitates and usually undesirable particles in the microstructure. Voids or pores are large regions without atoms and can be caused by gases or vacancy condensation in the solid state[22].

2.3 Formation process of $BaLa_4Ti_4O_{15}$

The formation process of BLT is defined by 4 consequent reactions and characterized by the formation of some intermediate phases:

$$La_2O_3 + 2TiO_2 \longrightarrow La_2Ti_2O_7 \quad (2\text{-}6)$$

$$La_2O_3 + TiO_2 \longrightarrow La_2TiO_5 \quad (2\text{-}7)$$

$$BaCO_3 + TiO_2 \longrightarrow BaTiO_3 + CO_2 \quad (2\text{-}8)$$

$$BaTiO_3 + La_2Ti_2O_7 + La_2TiO_5 \longrightarrow BaLa_4Ti_4O_{15} \quad (2\text{-}9)$$

The final equation, obtained by adding these four equations, is the following:

$$2La_2O_3 + BaCO_3 + 4TiO_2 \longrightarrow BaLa_4Ti_4O_{15} + CO_2 \quad (2\text{-}10)$$

The formation of $BaLa_4Ti_4O_{15}$ is the result of the combination of three different phases, $BaTiO_3$, $La_2Ti_2O_7$ and La_2TiO_5. BLT phase is formed at 1000 ºC and at temperatures above 1050 ºC is the only phase present when prepared by a molten salt method[23]. However, for powders prepared by solid state mixing this temperature is higher and at temperatures below 1300ºC other phases were detected[16].

2.4Sintering

2.4.1 Basics of sintering

Sintering is a processing technique that allows consolidating powder compacts using thermal energy. It´s used to obtain density-controlled materials with a large number of applications[8].

In ceramics (and metals) it is necessary to distinguish two types of structures: the crystal structure and the microstructure. The first is at an atomic scale and is related to the type of bonding. The second one is at a larger scale and it is related to the nature, quantity, and distribution of the structural elements or phases. These types of structures are related with intrinsic properties that depend on the microstructure. Intrinsic properties are properties like melting point and coefficient of thermal expansion which depends of the atomic bonding. On the other hand, properties as mechanical strength and relative permittivity are dependent on the microstructure. It is possible to change the microstructure (grain size, grain size distribution, density and size and distribution of other phases) through the sintering variables, such as temperature, heating rate, holding time, atmosphere and pressure[1,8].

Sintering could be divided into three categories: viscous flow sintering, liquid phase sintering and solid state sintering. Solid state sintering occurs when the compact is densified totally in the solid state at the sintering temperature. Liquid phase sintering occurs when the compact is sintered in the presence of liquid phase but this phase isn't enough to fill all the porosity. Viscous flow sintering takes place when liquid phase is enough to fill all space between the solid particles, and the full densification can be

achieved by a viscous flow of grain–liquid mixture without having any grain shape change during densification[8].

Solid state sintering is divided into three stages: initial, intermediate and final. In the first stage the compact shrinks 2-3% and this stage is characterized by formation of necks between particles. In the intermediate stage the compact achieves approximately 93% of relative density before close the pores. In the last stage the porosity is almost or totally eliminated[8].

2.4.1.1 Grain growth

Grain growth is the increasing of the grain size of a single-phase solid and occurs in dense and porous polycrystalline solids, at sufficiently high temperatures. The consequence is an increase in the average grain size and a decrease in the number of grains[1].

Polycrystalline microstructures are comprised of many single crystals (grains) joined together by a 3D network of internal interfaces (grain boundaries). Grain boundary corresponds to a lattice disorder region, between two crystalline regions, with an excess of free energy. Because of this, during the thermal and chemical etching these regions are preferentially removed. This excess of energy is the driving force for the grain growth. The grain boundary region has a width of approximately 0.5 to 1 nm (not known accurately)[1,24]. The heating of these polycrystalline microstructures promotes a coarsening of the grains and consequently a decrease of the grain boundary area[1,8].

The grain growth is divided into two types: normal and abnormal. Normal grain growth is better characterized in a single-phase system. Nevertheless, the kinetics varies from boundary to boundary, because of the differences in the grain boundary energy. The presence of a second-phase (Figure 3) hinders the grain boundary movement and, consequently, delays the grain growth[8]. The drag force of a particle against the boundary movement, F_d, is

$$F_d = \gamma_{gb} \sin\theta \times 2\pi r \cos\theta = \pi r \gamma_{gb} \sin 2\theta \quad (2\text{-}11)$$

where γ_{gb} is the grain boundary energy[1,8].

The grain boundary velocity (v_b) is approximately defined as the instantaneous grain growth rate [1]:

$$v_b = \frac{dG}{dt} \tag{2-12}$$

where G is the average grain size and t is the time. This parameter is also defined as the product of the driving force for grain boundary migration (F_b) and the boundary mobility (M_b) [1]:

$$v_b = M_b F_b \tag{2-13}$$

The grain boundary mobility is dependent on the atomic volume (Ω) and inversely dependent on the temperature (T) and grain boundary width (δ_{gb}):

$$M_b = \frac{D_a}{kT}\left(\frac{\Omega}{\delta_{gb}}\right) \tag{2-14}$$

where D_a is the diffusion coefficient for atomic motion across the grain boundary and k is Boltzmann constant.

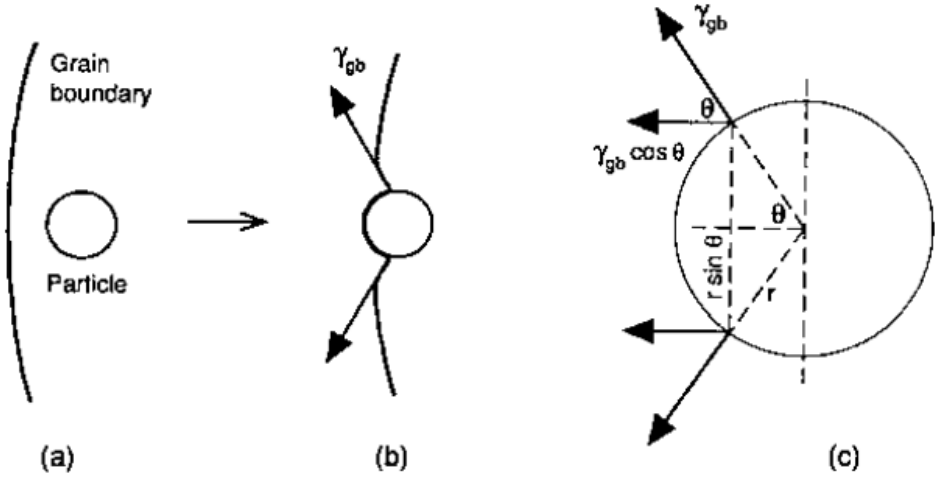

Figure 3 - Dragging of grain boundary movement by second-phase particles: the Zener effect. (a) Approach of the boundary toward the particle; (b) Interaction between the grain boundary and the particle leading to a retarding force on the boundary; (c) Detailed geometry of the particle - grain boundary interaction[1].

Grain growth happens when atoms diffuse from one side of the boundary to a new position on the other side. The movement of the atoms occurs from the "convex" surface to the "concave" one, as shown in Figure 4[1].

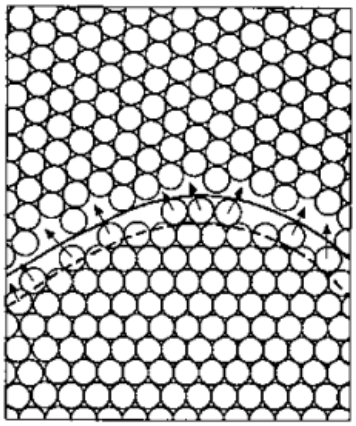

Figure 4 - Grain boundary and atoms migration from the "convex" to the "concave" side[1].

Grain boundary mobility depends on the material and may vary with the grain boundary orientation. Consequently, the grain growth, which is affected by the grain boundary mobility, cannot be rigorously analyzed. In order to understand the grain growth is used a classical theory and a constant grain boundary energy is assumed[8]. The classical mode was derived for bulk polycrystalline materials and is represented by the following equation:

$$\bar{G}_t^2 - \bar{G}_{t_0}^2 = \frac{4D_b^{\perp}\gamma_b V_m}{\beta RT\omega} T = \mathrm{KT} \qquad (2\text{-}15)$$

where $D_b^{\perp}$ is the atom diffusion coefficient across grain boundary, γ_b is the grain boundary energy, V_m is the molar volume, β is a proportional constant, R is the gas constant, T is the temperature, ω is the grain boundary thickness and t is the sintering time[8].

Normal grain growth

A normal grain growth promotes an increasing in the average grain size but with a grain size in the same range of values and similar shapes. The grain size distribution for

different sintering times is similar to the distribution shown in Figure 5. The initial and the final microstructure present a unimodal grain size distribution.

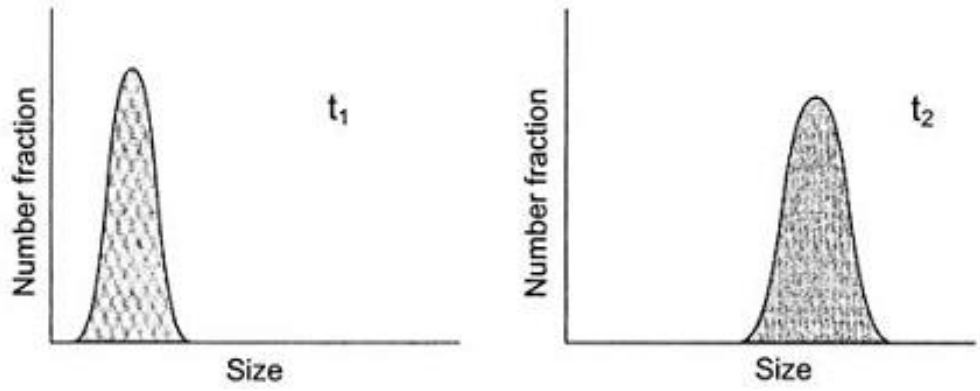

Figure 5 - Grain size distributions for two different sintering times (t1 and t2) and considering a normal grain growth[1].

Abnormal grain growth

In abnormal grain growth, some grains grow faster than the surrounding grains. In this case, the grain size distribution is different of the grain size distribution for normal grain growth. The initial grain microstructure is the same for the normal grain growth but the final presents a bimodal grain size distribution, as shown in Figure 6.

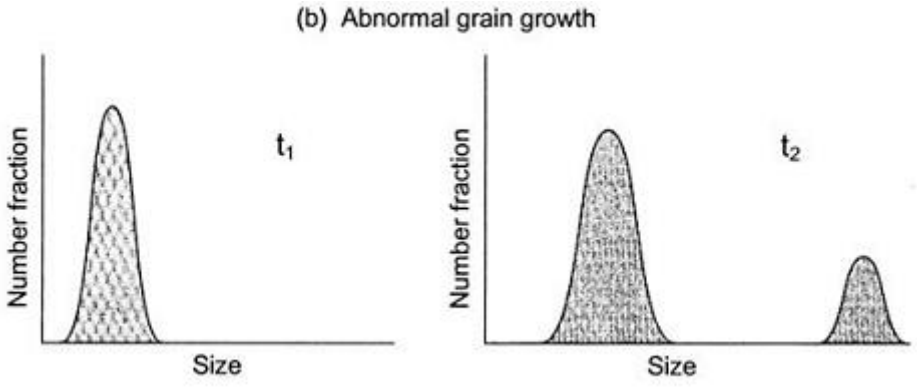

Figure 6 - Grain size distributions for two different sintering times (t_1 and t_2) and considering an abnormal grain growth[1].

2.4.2 Sintering studies and electrical properties of titanates

Titanates are an important family of materials with a wide range of applications. Because of its importance there are a large number of studies with sintering variables, such as sintering atmosphere, sintering temperature, composition and applied pressure.

2.4.2.1 Effect of the sintering temperature

The sintering temperature is an important sintering variable with effects on the characteristics of densified titanates.

L. C. Yan et al have sintered $SrTiO_3$ at temperatures between 1000 and 1400˚C with a temperature interval of 100˚C. It was observed no shrinkage at 1000 ˚C, shrinkage of 0.25% at 1100˚C and the highest shrinkage (10.35%) was achieved at 1400˚C. The authors have observed an influence of the temperature in the average grain size. An increase in grain size was detected with increase of sintering temperature. The relative permittivity and the losses were measured for these samples and the highest relative permittivity was observed in the sample sintered at 1200˚C, with a value around 50, and every sample have showed low losses with the frequency (<1)[25].

The effect of sintering temperature in electrical properties was also studied in $CaCu_3Ti_4O_{12}$ (CCTO). A variation in the electrical properties was observed in bulk samples sintered between 975 and 1100˚C, with a temperature interval of 25°C. The bulk and grain boundary permittivity increases with increasing the sintering temperature by a factor of 2 (approximately) and 300, respectively. In order to understand this variation in the electrical properties, an energy dispersive analysis of X-rays (EDAX) was performed. A chemical change was detected, such as segregation of Cu from the bulk in the grain boundaries, at 1050°C. The authors have concluded that the electrical properties of this system must be extremely sensitive to small chemical changes[26].

Variations in the relative permittivity and losses were observed in titanium dioxide (TiO_2) sintered at temperatures between 700 and 1000°C, accordingly with the changes in the microstructure. As expected, the density and the grain size increases with the increasing temperature. A relative density (with respect to the theoretical density) of

92.5%, approximately, was achieved at 700°C and for 1000°C the TiO_2 samples are almost full densified. The grain size for the sample sintered at the higher temperature was 18 times the grain size of the sample sintered at the lowest temperature. The grain size distribution was also affected: for lower temperatures a uniform grain size was observed but for the higher temperatures a bimodal distribution was detected[27]. The dielectric measurements were performed for samples sintered at 700, 800, 900 and 1000°C. The relative permittivity of the samples sintered at 900 and 1000°C shows a strong dependence on the measuring frequencies. The highest relative permittivity was achieved for the sample sintered at 900°C at 1Hz, decreasing to a plateau of 133 for higher frequencies, as it is possible to see in Figure 7 (a). The loss tangent shows a peak for the samples sintered at 900 and 1000°C, unlike the samples sintered at lower temperatures that are more stable with the frequency[27].

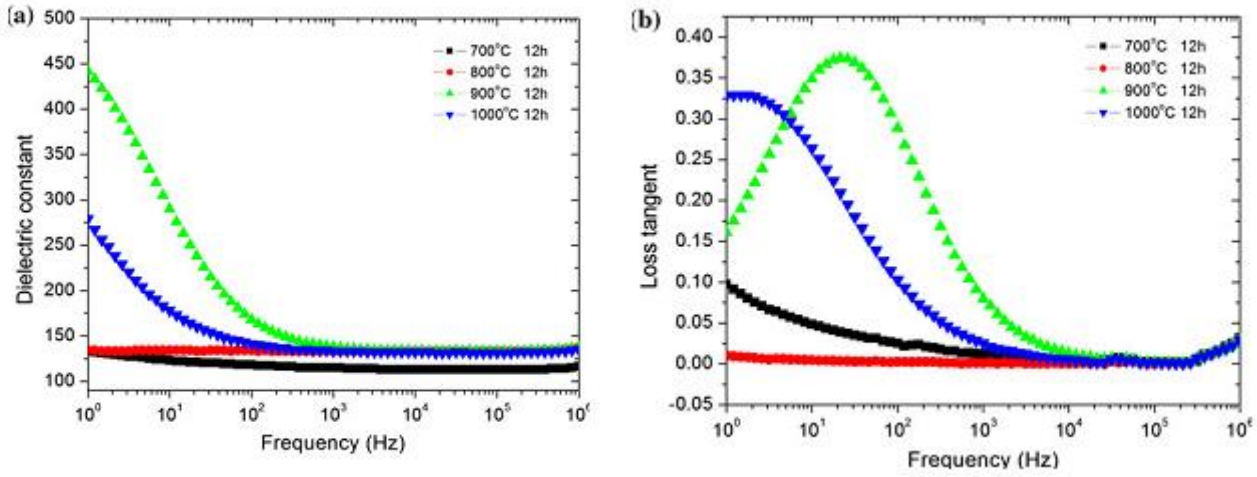

Figure 7 - (a) Relative permittivity and (b) loss tangent of TiO_2 samples sintered at different temperatures[27].

2.4.2.2 Effect of the sintering atmosphere

The effect of the sintering atmosphere on the properties of some titanates has been studied in the last years. Chung *et al*[7] examined the effect of the sintering atmosphere on grain boundary segregation and grain growth in niobium-doped $SrTiO_3$. Samples were sintered in reducing (dry H_2) and oxidizing (air) atmospheres. The authors have concluded

that Niobium segregation occurs in a reducing atmosphere and two different grain boundaries were observed: one without an intergranular phase, as the sample sintered in air, and other with intergranular phase. The grain growth is slower in the reducing atmosphere than in the oxidizing one[7].

Other study was performed to study the effect of the sintering atmosphere on the electrical properties and the chemical properties of the grain boundaries. $SrTi_{0.99}Nb_{0.01}O_3$ was sintered in three different atmospheres: air, nitrogen (N_2) and nitrogen-hydrogen (N_2-H_2). With these variations, the grain boundary resistivity varies from 0.12 to 130 MΩ.cm, but the grain resistivity remains several Ω.cm. The ratio of O/(Ti+Sr) near to the grain boundaries increased when the atmosphere was changed from nitrogen-hydrogen to air[28].

The effect of sintering atmosphere was studied by Li et al during sintering of $SrTiO_3$. This titanate was sintered in reducing atmospheres with 25% N_2 + 75% H_2, 50% N_2 + 50% H_2 and 70% N_2 + 30% H_2. It was observed that the measured capacitance at 1 kHz increases with the increasing of H_2 content, as shown in Figure 8. An explanation to this, it's that a reducing atmosphere lead to more free electrons during the sintering process and a thinner oxidation layer is introduced and, consequently the capacitance increases. When a weak reducing atmosphere is used to sinter, higher temperatures are needed to have a semiconducting behavior in $SrTiO_3$. Increasing the H_2 content, lower temperatures are needed to achieve the same electrical response. In addition, the grain size shows the same trend and increases also with the increasing of the H_2 content[29,30].

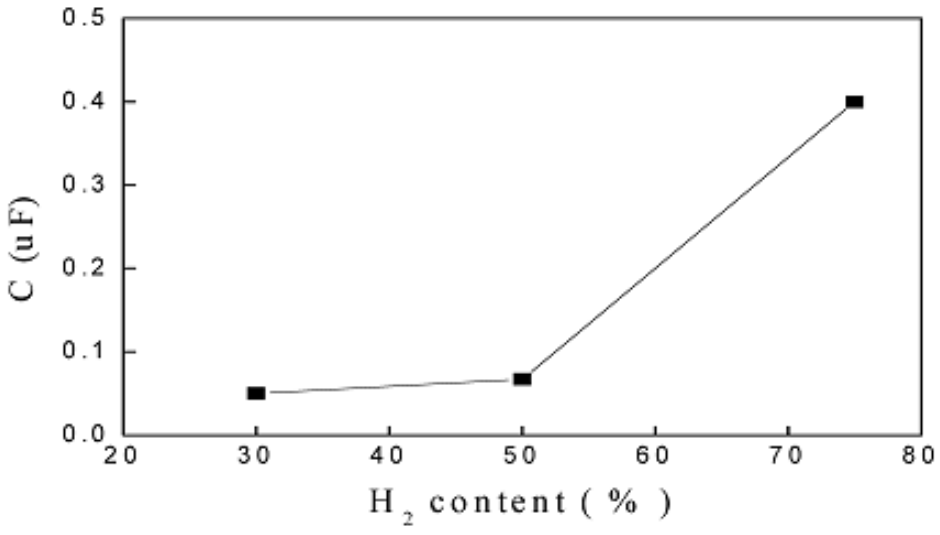

Figure 8 - Capacitance measured at 1kHz for samples sintered in atmospheres with different H_2 content[28].

The structural transition of grain boundaries between faceted and rough in 0.1 mol% TiO_2 excess $BaTiO_3$ was studied in samples sintered at 1250˚C by 50h in atmospheres with oxygen partial pressure (pO_2) between ~0.2 atm (air) and ~10^{-19} atm (H_2). The grain growth behavior and the grain boundary structure are dependent on the pO_2 (Figure 9).

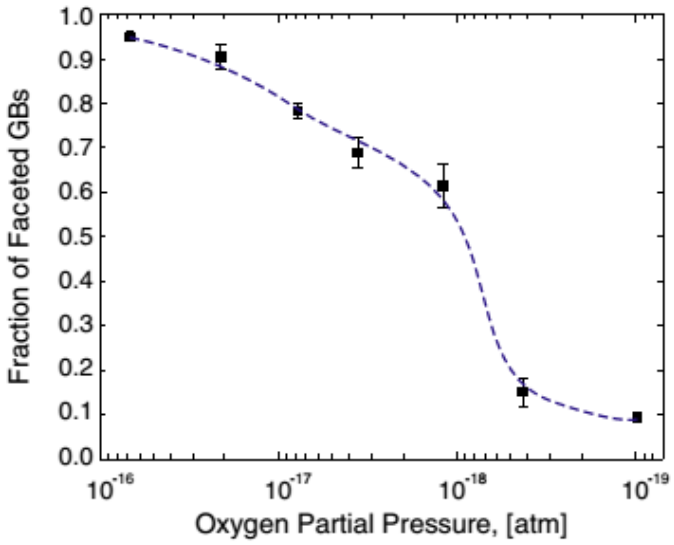

Figure 9 - Fractional variation of faceted grain boundaries of 0.1 mol%-TiO2-excess BaTiO3 sintered at 1250°C for 50 h with respect to the oxygen partial pressure [31].

At pO_2 = 0.2 atm the boundaries are all faceted (Figure 10 (a)), at pO_2 = $4x10^{-18}$ atm are partially faceted (Figure 10 (b)) and at pO_2= $9x10^{-20}$ atm the grain boundaries are mostly rounded (Figure 10 (c)). The systematic change in oxygen partial pressure resulted in an evolution of the grain boundary structure between faceted and rough, which result in a different growth behavior. This could be related with the step free energy of each faceted boundary that decreases with the oxygen partial pressure reduction. Grain growth was suppressed in samples sintered with pO_2 between 10^{-11} and 10^{-17} atm (defaceted grain boundaries)[31].

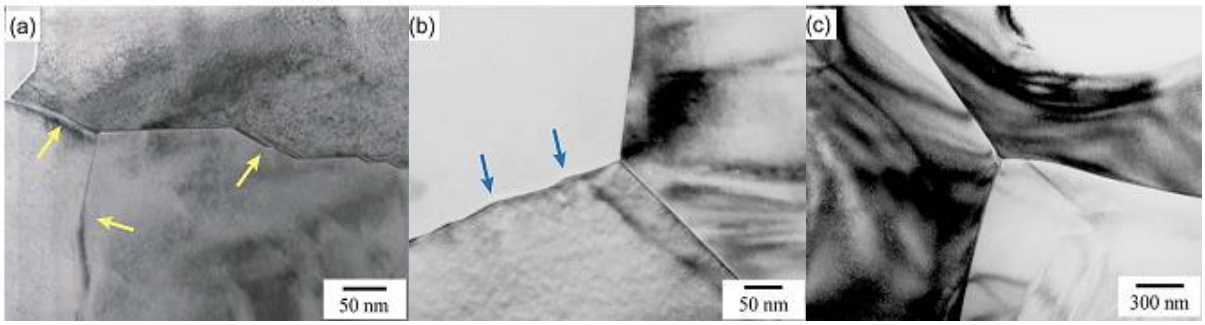

Figure 10 – TEM microstructures showing grain boundary morphology sintered under pO_2 of (a) 0.2 atm; (b) $4x10^{-18}$ atm and (c) $9x10^{-20}$ atm[31].

2.4.2.3 Effect of the applied pressure

Calcium cooper titanate ($CaCu_3Ti_4O_{12}$ or CCTO) is a material with good properties for microelectronics applications. Kim *et al* have prepared samples of CCTO by hot pressing, at a pressure of 15 MPa, at 1100 ˚C for 1 h or 3 h. Additionally, identically samples were prepared by conventional sintering, at the same temperature with holding time between 1 and 16h, and were used for comparison. The authors reported a dielectric response dependent on the holding time and the type of processing[32] .

Samples which were obtained through conventional sintering have an effective permittivity of ~4000 and this value was almost independent of the frequency range. Samples that were hot pressed showed a gradual reduction of the effective permittivity with increasing frequency above 10^4 Hz, but an unusually high value for grain size were observed ($3x10^4$ for 1 kHz). For the samples prepared by conventional sintering, grain and grain-boundary resistivities show a decrease with the increasing of the holding times. In the hot pressed samples there is no influence of holding time in the resistivity. According to the equation (2-16), a higher relative permittivity of the grain boundary (ε_{gb}) and a thin grain boundary (δ_{gb}) in the hot pressed samples may be responsible for the higher value of effective permittivity (ε_{eff}) for the hot pressed samples [32].

$$\varepsilon_{\text{eff}} \approx \varepsilon_{gb} \frac{A}{\delta_{gb}} \tag{2-16}$$

The existence of a CuO phase may be responsible for the lower values of effective permittivity in samples prepared by conventional sintering.

BLT thick films show a similar effect when sintered in a platinum substrate and a densified BLT substrate. Elongated grains were observed in samples sintered at 1500˚C with a heating rate of 25˚C/min until 1400 ˚C and 7˚C/min between 1400˚C and 1500˚C, with variation of the isothermal time (0 to 180 min)[2].

In Figure 11 it is possible to observe a delay in the densification between films and bulk samples, but after 180 minutes of isothermal time both samples achieved the same densification.

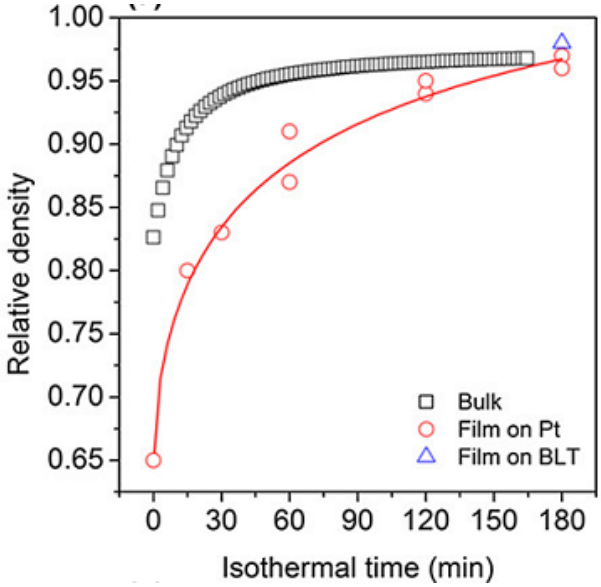

Figure 11 – Relative density as a function of isothermal time[2].

The observation of the microstructures reveals, for the same conditions, a larger grain size in films on BLT substrate than for bulk samples (Figure 12). The microstructures also show elongated grains for films and bulk. Although, for bulk samples, the elongation degree is lower than for films. This could be related to the stresses induced by the constraint of the substrate during sintering which may increase the grain boundaries mobility or the driving force for transport enhancing the grain growth.

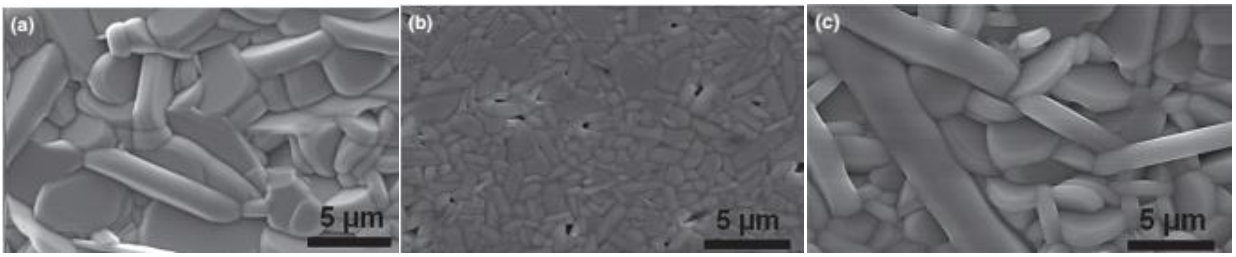

Figure 12 – SEM micrographs of BLT samples sintered at 1500°C for 180 min: (a) film on Pt (top view); (b) bulk (polished fracture surface); and (c) film on BLT (top view) [2].

A study of Besson and Abouaf[33,34] in alumina may help explaining other study made by our investigation group in BLT thick films[2]. In the alumina study, samples were prepared by Hot Isostatic Pressing (HIP) at 1300 ˚C with different pressures and holding times. Samples conventionally sintered were also prepared. The final densities obtained are in most cases 99%, but for lowest and highest pressure, 20 and 200 MPa, respectively, are less effective for the densification (Figure 13)[33].

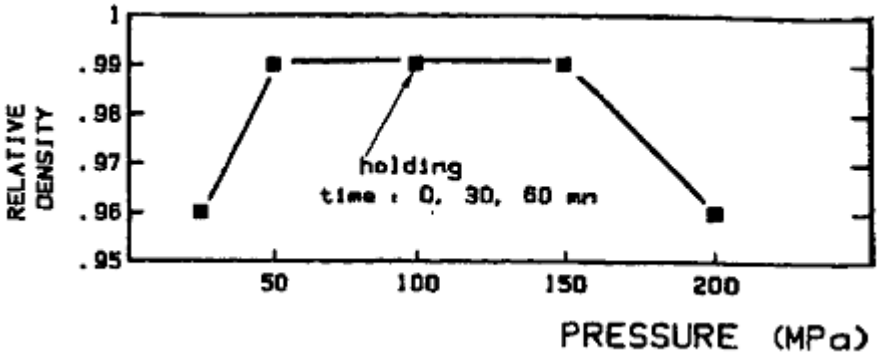

Figure 13 – Density as a function of HIP pressure (holding time 60 min, 1300˚C)[33].

The grain size observed after a HIP cycle is a linear function of the applied pressure (Figure 14). The authors observed an abnormal grain growth under 200 MPa and this could be the explanation for the lower density at this pressure.

The grains shape was observed and was used a shape factor, F_g, in order to estimate the shape changes of grains. The shape factor is defined by:

$$F_g = \frac{\pi}{4}\frac{D_g^2}{S} \tag{2-17}$$

where D_g is the geodesic diameter and S is the area of the particle. The shape factor is equal to 1 for a circle[33].

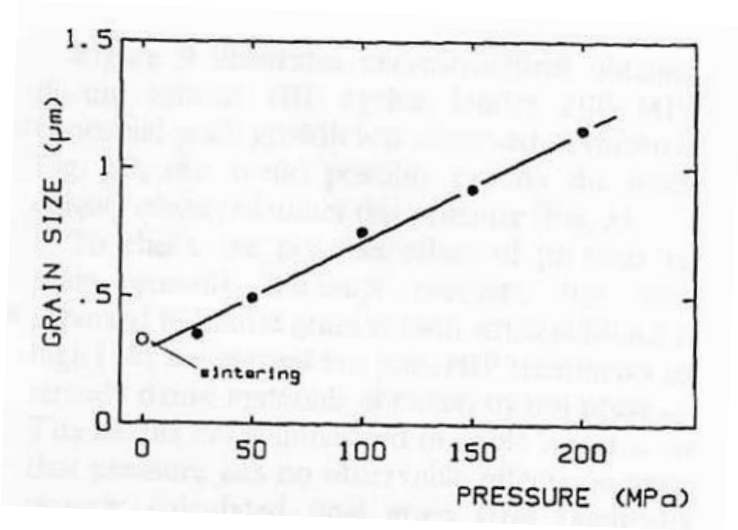

Figure 14 – Final grain size after HIP (holding time 60 min, 1300˚C) as a function of pressure[33].

It was observed variations of the shape factor with the sintering time. Initially the particles have worm-like shape and with sintering time they become rounded, but for long sintering time grain growth along a specific crystallographic direction can occur and originate elongated grains with an increasing in the shape factor, as shown in Figure 15 (a). For samples prepared by HIP it is possible to conclude that increasing the pressure promotes the rounding of the particles, but a sufficiently high pressure (<150 MPa) stimulates an anisotropic grain growth with elongated grains[33].

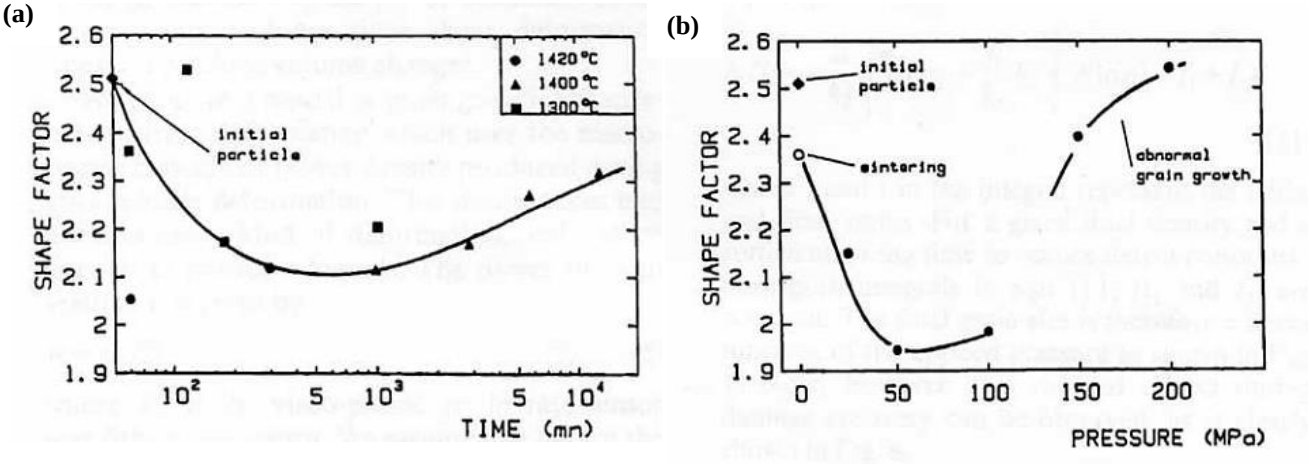

Figure 15 – Mean shape factor during (a) sintering as a function of time and (b) HIP (holding time 60 min, temperature 1300˚C) as a function of pressure [33].

Other study of Besson and Abouaf[34] with samples prepared in the same conditions, in HIP, shows that pressure has no effect on densified samples and grain growth enhancement was not observed. A hot pressed sample (130 MPa, 1300 ˚C, 1h) was prepared and the grain growth enhancement was also observed and the microstructure is similar to the microstructure obtain for the sample obtained by HIP at 150 MPa.

These studies show the importance of the applied pressure during sintering on the grain growth and properties of the grain boundaries and, consequently, on the electrical properties.

Chapter 3

Experimental procedure

This chapter presents the experimental procedure used to prepare and characterise BLT ceramics and precursors. BLT powders were analysed by XRD, in order to check if the powders are monophasic and if we have obtained the desired phase; by Coulter to know the particle size of the powders; and by Scanning Electron Microscopy to observe the particle morphology. A dilatometric characterization in different atmospheres was done in order to study the sintering behaviour of BLT powders. After sintering all samples were characterized: grains size, grain size distribution and grain aspect ratios were done with SEM images and using the Image J software; relative permittivity, dielectric losses, conductivity and temperature coefficient of relative permittivity were measured to electrical characterization.

3.1 Powder and samples preparation

$BaLa_4Ti_4O_{15}$ powders were prepared by conventional solid state oxide mixing. The precursors TiO_2 (Merck), La_2O_3 (Merck) and $BaCO_3$ (Merck) were weighted according to their stoichiometric proportions. Powders were then mixed in a ball planetary mill in ethanol for 24 h at 180 rpm, using Teflon pots with zirconia balls. After that, the slurry was dried in an oven, at 90 °C, for more than 12 h.

The powders were calcined in alumina crucibles at 1330 °C for 3 h.[16] During calcination the reaction (2-10) occurred.

After the calcination step powders were ball milled to reduce the particle size up to 0.715 μm, during 24 h at 180 rpm again and dried under the previously mentioned conditions.

Bulk samples were prepared by uniaxially pressing at 500 MPa during 30 s and then cold isostatically pressed (CIP) at 250 MPa during 1 min.

3.2 Powder characterization

The phase formation in BLT was checked by X-Ray Diffraction (XRD) analysis at room temperature in a powder X-ray diffractometer (Rigaku D/Max-B, Cu Kα). The diffraction angle was varied in the range of 10-80° and the scanning rate was 3°/min.

The particle size after ball milling was determined by using Particle Size Analyzer (Coulter LS230) in a water medium. The analysis was performed in suspension with concentrations of 1 g/l.

The morphology of BLT powders was assessed by Scanning Electron Microscopy (SEM) using an Hitachi, S-4100 SEM/EDS. For SEM observations, 1 g of BLT powder was dissolved in 50 ml of ethanol (pro-analysis) and ultrasonicated for 10 minutes. A drop was placed in the holder and dried for 1h at 90 ºC.

3.3 Dilatometric characterization

The sintering behavior of BLT powder was assessed by dilatometric analysis. Dilatometries were performed in a computer assisted vertical dilatometer (Linseis, mod. 4 L70-2000) heating the samples from room temperature to 1550ºC, with a heating rate of 7ºC/min. Parallelepipedic bars of milled BLT powders of 9 x 4.5 x 4.5 mm were pressed at 500 MPa during 30 s and then cold isostatically pressed (CIP) at 250 MPa during 1 min.

Dilatometries were performed using three different atmospheres, argon, oxygen and air.

3.4 Sintering conditions for grain boundary studies

CIP samples were sintered in three different atmospheres, N_2, O_2 and air in a horizontal tubular furnace (alumina tube). The sintering temperature was 1530 °C and the heating rate was 7 °C/min. The holding time varied between 0h and 10h for each sintering atmosphere. The sintering temperature was defined by the dilatometric analysis.

6 samples were sintered in N_2, 6 samples were sintered in O_2 and 2 samples were sintered in air, in a total of 14 samples. All samples were sintered in an alumina sample holder.

3.5 Density meaurements

Samples density was measured before and after each sintering cycle. In the green state the density (d) was measured by the geometrics' method, using the equation (3-2):

$$d = \frac{m}{V} \text{ (g/cm}^3\text{)} \quad (3\text{-}2)$$

where m is the mass of the sample in grams (g) and V the volume of the sample in cm^3.

The density of the sintered samples was measured by the Archimedes' method using water as the immersion liquid. The value of density was calculated using the following equation[35]:

$$d = \frac{d_{liq}W_1 - d_{air}W_2}{W_1 - W_2} \text{ (g/cm}^3\text{)} \quad (3\text{-}3)$$

where d_{liq} and d_{air} are the density of the liquid and the air, respectively, at the room temperature at 1 atm (d_{liq} = 1g/cm^3 and d_{air} = 0.001185 g/cm^3); W_1 and W_2 are the weight of the sample in air and in liquid, respectively.

The theoretical density value of 6,195 g/cm^3 for BLT was considered in order to calculate the relative density [16].

3.6 Microstructure characterization

For the microstructure characterization fractured and polished surfaces of all the sintered samples (under different atmospheres and pressures) were observed by Scanning

Electron Microscopy (SEM) and energy dispersive spectroscopy analysis conducted using an Hitachi, S-4100 SEM/EDS. For these observations all sintered samples were polished in 400#, 1000# and 1200# silicon carbide (SiC) grinding paper and then with diamond paste of particle size between 6 and ¼ µm up to shinning surfaces were obtained. After polished the samples were thermally etched at 1480 °C for 1 minute to contrast the grain boundaries. The preferential etching of grains boundaries was confirmed in an optical microscope (Nikon, HFX-IIA). Before the observation a carbon thin layer was deposited on the samples surface using a carbon depositor (Emitech K950X).

3.7 Grain size measurements

Using the SEM micrographs and Image J software[36] for images analysis, parameters like grain area, grain orientation and aspect ratio were determined. SEM images were modified in order to achieve binary images, as shown in Figure 16. The image contrast and brightness were improved in order to obtain a better difference between grain boundaries and grains. Grain boundaries were carefully observed and manually drawn, one by one, and images similar to Figure 16 (b) were obtained. After this image treatment was applied the thresholding and all mentioned parameters measured with the Image J software[36] (with calibrated images). More than 1000 grains were analyzed for each sample, which are 5 or 6 images per sample depending on the image magnification.

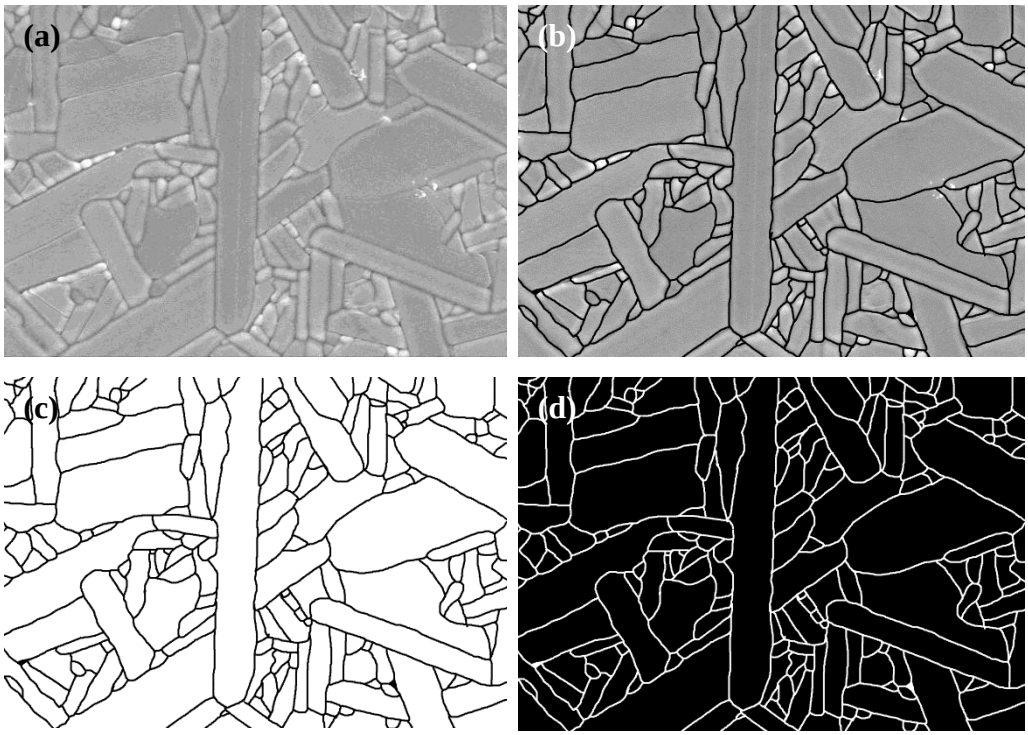

Figure 16 - Image processing according to image J software[36] for microstructure characterization (a) raw image, (b) grain drawing, (c) grains binarization and (d) inverted image.

3.8Dielectric characterization

The dielectric properties were measured as a function of temperature and frequency in a capacitive cell as the illustration in Figure 17. The current discharge flow of the capacitive cell, with the applying of a sinusoidal voltage (U) is given by the equation:

$$I = \frac{i\omega\varepsilon^* U\varepsilon_o S}{d_s} = \frac{i\omega(\varepsilon' - i\varepsilon'')U\varepsilon_o S}{d_s} = I_C + I_R \quad (3\text{-}4)$$

where *i* is the imaginary operator, $\omega = 2\pi f$ for the angular frequency, $\varepsilon_o$is the vacuum permittivity, S is the area of electrode, d_s is the samples thickness (or distance between electrodes), ε^* is the complex permittivity, $\varepsilon'$is the real part of the permittivity and $\varepsilon''$is the imaginary part of the permittivity.

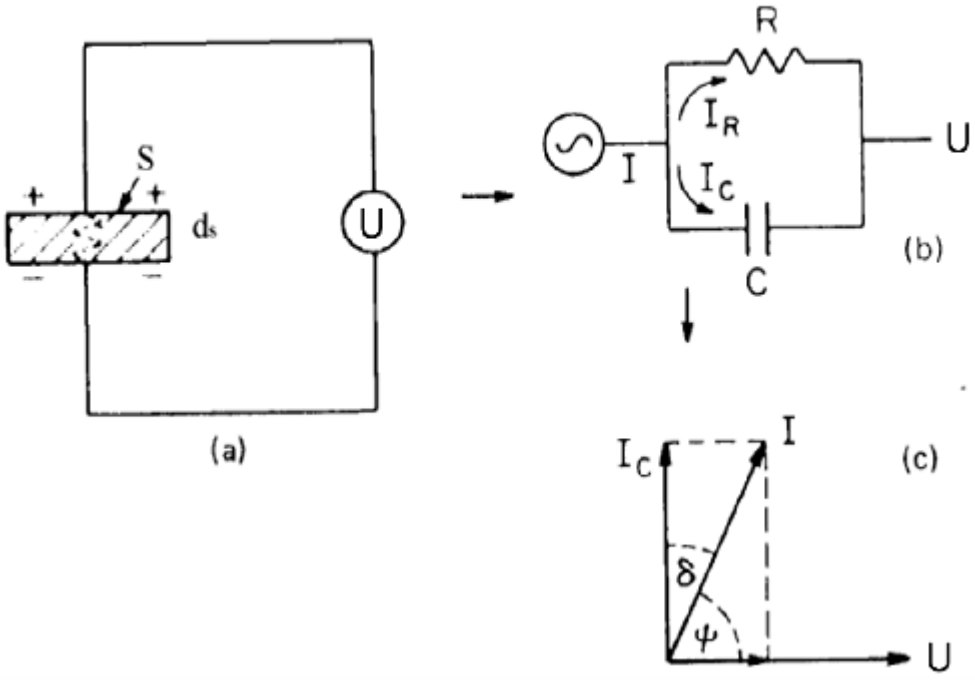

Figure 17 - Equivalent circuit diagrams of capacitive cell (a) of charging and loss current (b) and of loss tangent for a typical dielectric (c) .

The electrical properties were evaluated using an impedance bridge (HP 4284A Precision LCR Meter Agilent, USA) using frequencies between 20 Hz and 1 MHz in a temperature range of 30 and 400ºC .

Chapter 4

Results and discussion

This chapter presents and discusses the results obtained from the sintering studies conducted on BLT under different sintering atmospheres. Because sintering and microstructure development depend on the morphology of the starting powders, these results are firstly presented and discussed. Finally for the electrical behavior selected samples are characterized.

4.1 Powder characterization

Figure 18 shows the X-ray diffraction patterns of $BaLa_4Ti_4O_{15}$ calcined powders. According with the detection limit of the equipment a monophasic $BaLa_4Ti_4O_{15}$ powder could be obtained after calcination at 1330 ºC for 3 h.

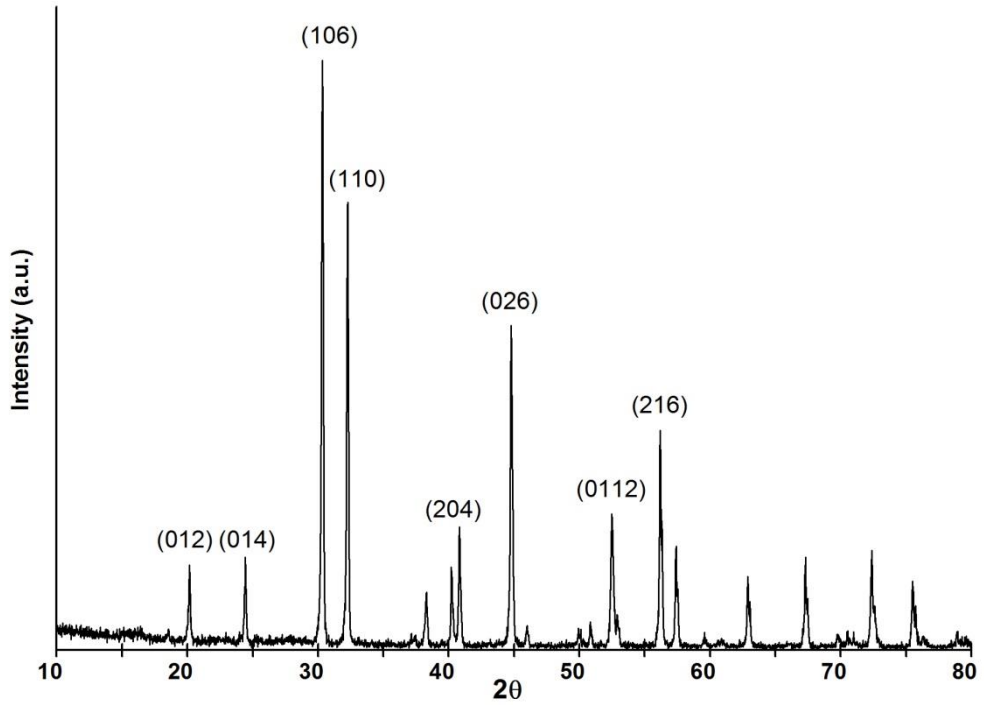

Figure 18 – XRD spectra for BLT powders after calcination, presenting a monophasic BLT powders. The main diffraction peaks are identified.

Figure 19 depicts the particle size distribution for BLT powders obtained by laser diffraction (Coulter) after ball milling for 24h at 180 rpm, calcination at 1330 ºC for 3 h and ball milling again in the same previous conditions. A bimodal distribution is presented with modes centered at 0.2 µm and 1.75 µm respectively. A particle size below 4 µm was obtained and the average particle size for these powders was 0.715 µm and the median size was 0.368 µm.

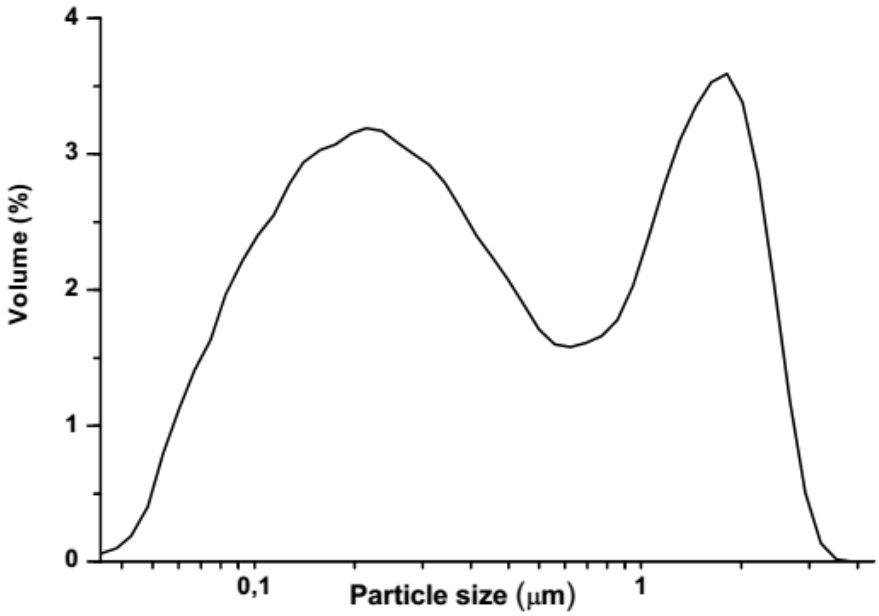

Figure 19 – Particle size distribution for calcined BLT powder. A bimodal distribution is observed, with an average particle size of 0.715 µm.

The obtained particle size distribution is similar to the bimodal distribution obtained in another studies [16,37], and the median particle size is similar to the particle size for BLT powders prepared in the same conditions, obtained in a previous study [16].

The morphology of calcined and milled BLT powders was observed by SEM and Figure 20 depicts a representative microstructure. The particles have a non-spherical, parallelepipedic shape somehow related with the hexagonal BLT cell. The crystal structure allows the particle elongation due to the great difference between the lattice parameters (a = 5.5671 Å and c = 22.4602 Å). Particles with different sizes are visible in the image. The

particle size was calculated using the SEM images and Image J software in order to compare with the grain size obtained by laser diffraction. An equivalent diameter of 0.99 μm was calculated.

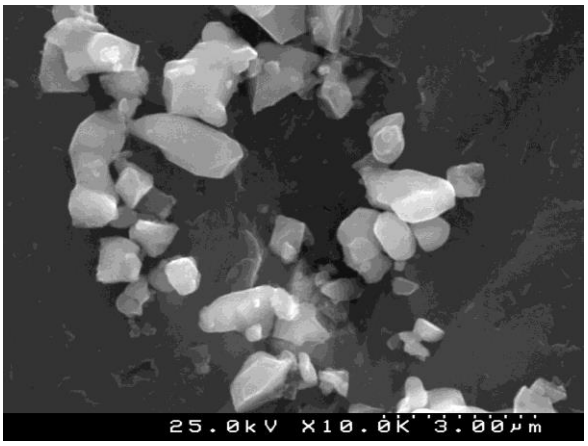

Figure 20 – SEM micrographs of a set of BLT particles with a non-spherical cubic shape.

4.2 Sintering behavior

Dilatometric analyses were conducted to follow the sintering of BLT and the effects of the sintering atmosphere on the shrinkage curve. Three different atmospheres were used: O_2, air and argon. An argon atmosphere (reducing) was used instead of a nitrogen atmosphere, because nitrogen was not available to do this experiment. The shrinkage curves obtained at 7ºC min^{-1} were represented in Figure 21 and the respective derivative curves in Figure 22.

For all the tested sintering atmospheres high sintering temperatures, larger than 1500ºC, are needed to attain high shrinkage values. Though similar dilatometric curves were obtained in terms of sintering temperatures and shrinkage, some differences as a function of the atmosphere can be deppicted. The derivative curves in Figure 22 show that the shrinkage rate in function of the temperature is very similar for the samples sintered in air and argon, but a higher shrinkage rate is obtained in oxygen. Samples sintered in argon also starts to shrink at a slightly higher temperature than when sintered in atmospheres with oxygen (see table 2). Consequently, the shrinkage obtained at 1530ºC is highest in O_2 and lowest in argon. From these results we can assume that pO_2 will influence the mass

transport for shrinkage and/or coarsening during sintering, which will be further evaluated in the microstructural features of sintered samples presented in next section.

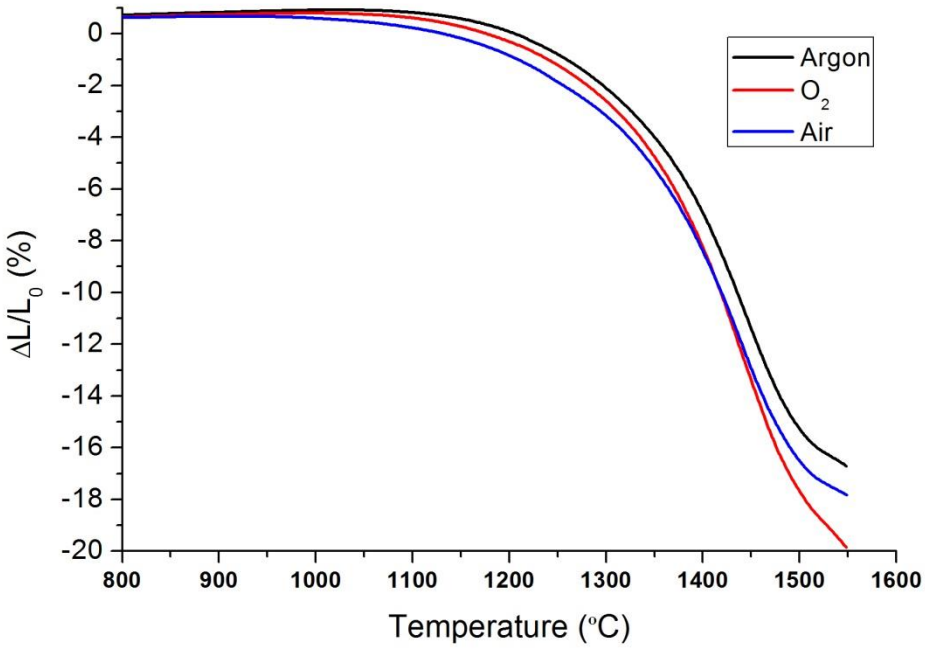

Figure 21 – Dilatometric curves for BLT in argon (black line), oxygen (red line) and air (blue line). At 1550 ºC oxygen presents the higher shrinkage.

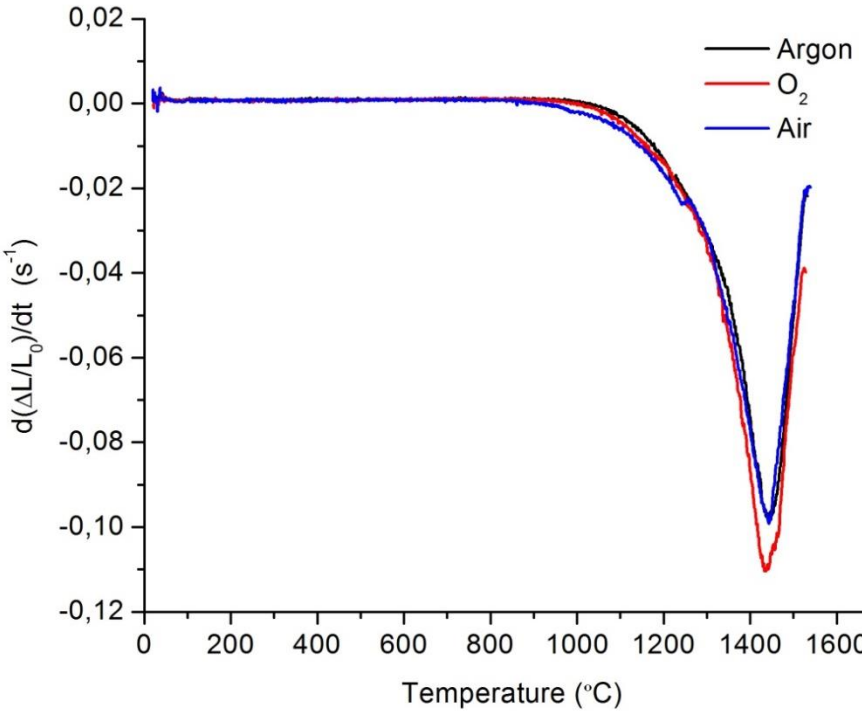

Figure 22 –Derivative of dilatometric curves for BLT in argon (black line), oxygen (red line) and air (blue line).

Table 2 – Start shrinkage temperature (T_s), temperature for the maximum velocity (T_{max}), maximum velocity (V_{max}) and total shrinkage at 1530ºC (S_{1530}) for the three atmospheres.

Atmosphere	Ts (°C)	Tmax (°C)	Vmax (s^{-1})	S_{1530} (%)
Oxygen	~984	1434	-0.11	19.1
Air	~860	1442	-0.10	17.5
Argon	~1010	1438	-0.10	16.3

4.3 Characterization of sintered compacts

4.3.1 Structural

4.3.1.1 X-Ray diffraction for sintered pellets

After sintering, pellets were crushed and turned into powder to perform XRD analysis. A second phase was found in samples sintered in oxygen and nitrogen, nevertheless in small amounts.

The second phase present in oxygen sintered samples is a lanthanum titanate ($La_2Ti_2O_7$) and is detected in samples sintered between 1 hour and 10 hours (Figure 23).

A different second phase was found in samples sintered in nitrogen, a barium titanate (Ba_2TiO_4) (Figure 24). This phase appears in samples sintered between 30 minutes and 10 hours.

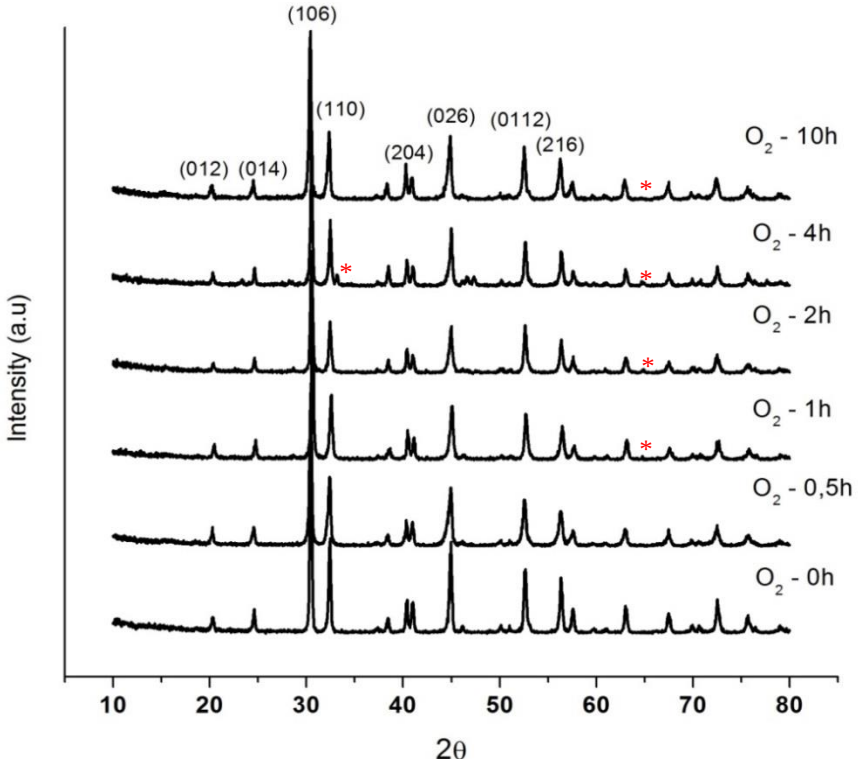

Figure 23 – XRD spectra for samples sintered in oxygen at 1530°C with different isothermal times with the peaks corresponding to the $La_2Ti_2O_7$ phase (*). This phase appears for the diffraction angles (2θ) of 63º for samples sintered between 1 and 10 h and 33º for sample sintered during 4 h.

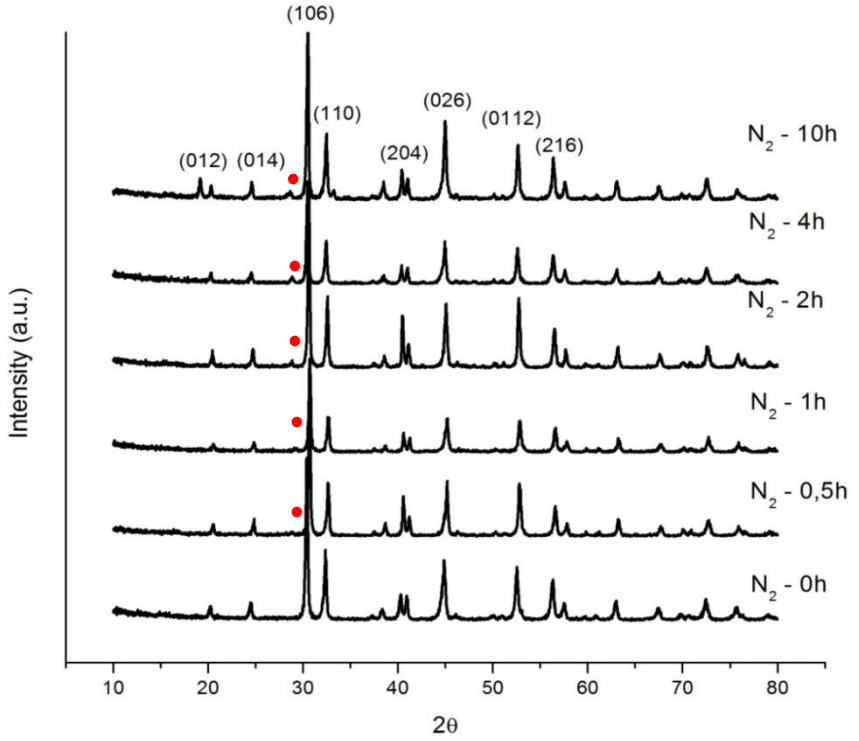

Figure 24– XRD spectra for samples sintered in nitrogen at 1530°C with different isothermal times, with the peaks corresponding to the Ba_2TiO_4 phase (•).This phase appears for the diffraction angle (2θ) of 29º for samples sintered between 30 min and 10 h.

4.3.2 Microstructural

The density of green compacts was measured by the geometrical method and density of 58±1% was obtained.

The density of the sintered compacts was measured by the Archimedes method (table 3). Figure 25 represents the samples density after sintering at 1530ºC in three different atmospheres as function of the sintering time. As the sintering time increases the relative density increases and values above 92% were observed. In these curves, independently on the sintering atmosphere two main regions can be observed; in oxygen, initially the relative density increases with the sintering time in an almost linear way until 2 h of sintering time; after that the increase in the relative density is not linear and the density tends to a constant value around 100%; in nitrogen, the relative density increases fast until 2h and slowly for larger sintering times.

As expected from the dilatometric curves presented in Figure 21, in oxygen atmosphere a higher relative density was achieved, almost 100% for a sintering time of 10 hours and for the same sintering time the lowest obtained density was 97 % for nitrogen atmosphere.

Table 3 – Relative density, average grain area, relative variance for the grain area distribution and average aspect ratio for samples sintered in N_2, O_2 and air at 1530ºC between 0 and 10 h.

	Time (h)	Relative density (%)	Average grain area (μm^2)	Relative variance	Average aspect ratio
N_2	0	91.6	1,92	6.52	2.43
	0.5	91.8	2,48	8.60	2.50
	1	92.4	2,69	14.28	2.51
	2	95.4	2,73	55.42	2.68
	4	96.2	2,48	54.61	2.58
	10	97.0	2,79	106.59	2.78
O_2	0	96.7	2.04	6.93	2.45
	0.5	97.1	2.34	12.06	2.68
	1	98.6	2.55	17.02	2.66
	2	99.5	2.75	41.07	2.85
	4	99.5	2.74	47.20	2.86
	10	99.7	4.19	139.37	2.91
Air	0	95.5	1.98	6.75	2.41
	10	99.0	3.62	72.36	2.86

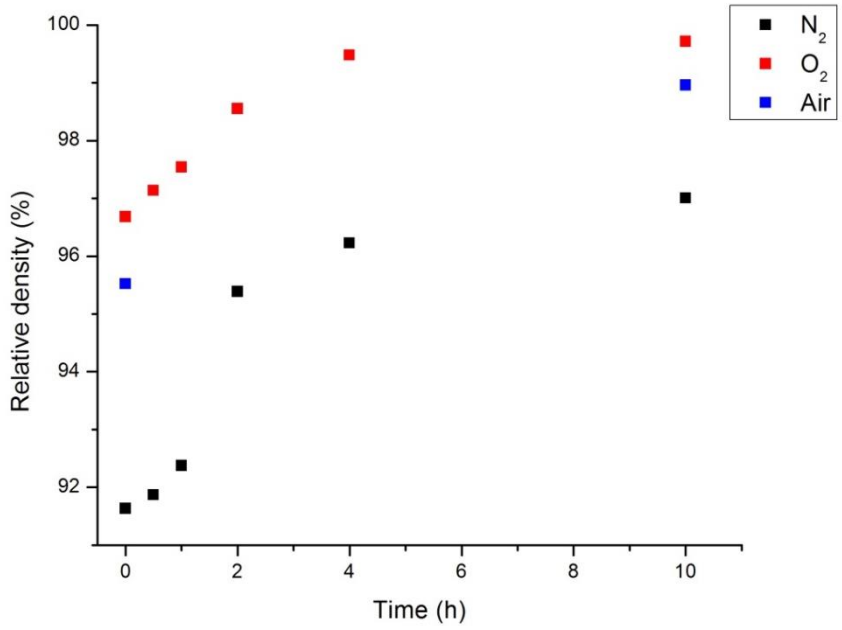

Figure 25– Density versus time for samples sintered at 1530°C in nitrogen (black squares), oxygen (red squares) and air (blue squares). Higher densities were achieved in an oxygen atmosphere.

The samples sintered in oxygen shown in Figure 26 dense microstructures with residual porosity mainly located at the grain boundaries. Exception is made for the sample sintered for 10h where very few intragranular pores can be observed inside the larger grains. The microstructures are characterized by elongated grains and as the sintering time increases an abnormal grain growth occurs with very big elongated grains embedded in a matrix of smaller elongated grains (Figure 26(d)).

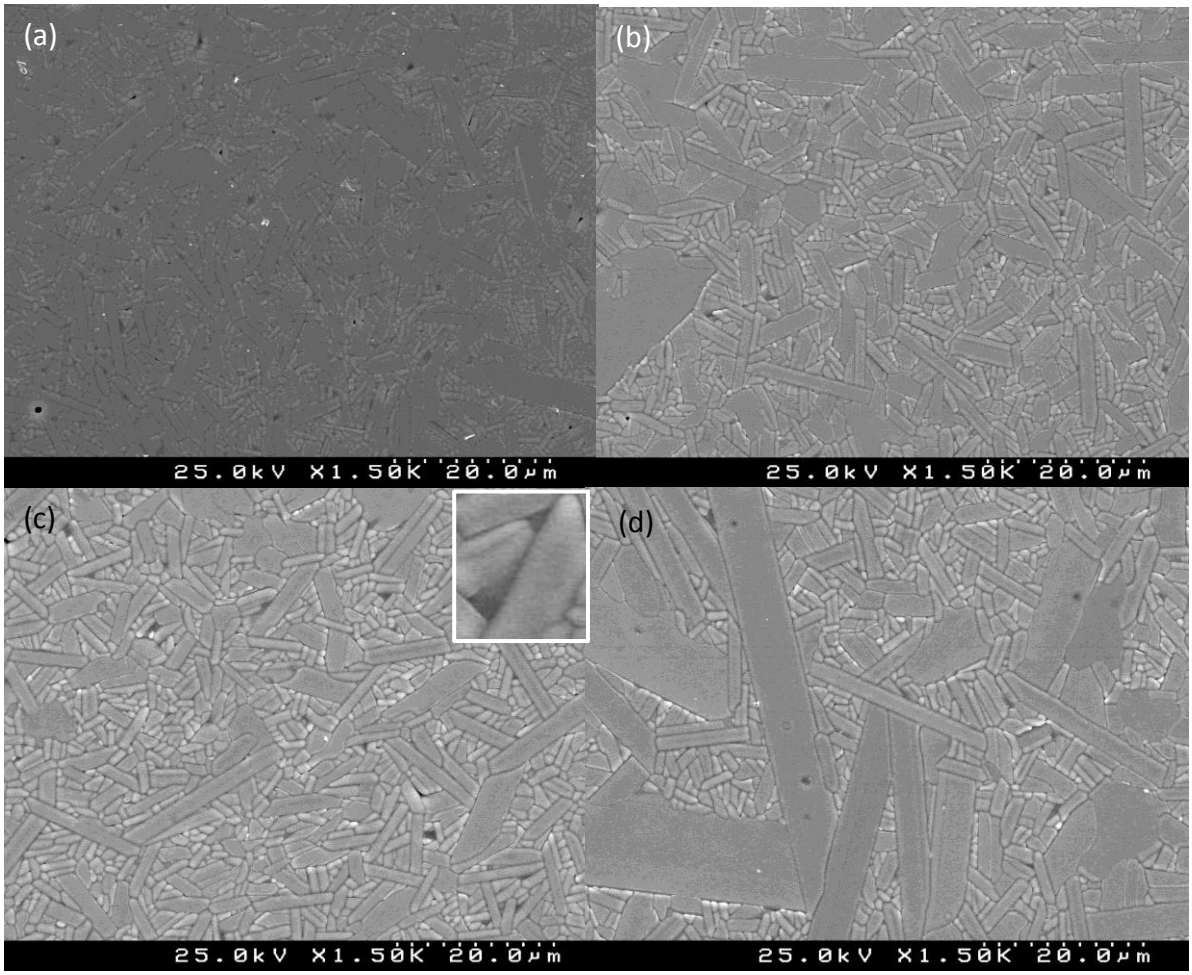

Figure 26 – SEM images of sample sintered in O_2 at (a) 0 hours, (b) 1 hour, (c) 2 hours (inset shows the presence of a second phase) and (d) 10 hours (the magnification is the same for all images). All the samples show dense microstructures with residual porosity located at the grain boundaries. The microstructures are characterized by elongated grains and an abnormal growth with very big elongated grains embedded in a matrix of smaller elongated grains. As the sintering time increases the abnormal grain growth becomes more obvious with bigger grains.

The grain elongation was promoted by the anisotropic crystal structure of BLT, which grows along the preferred c-axis orientation [38]. However, grains excessively large are found for longer times, as it is possible to see in Figure 26 (d). With the increasing the isothermal time the grain area distribution becomes larger as shown in Figure 27 and qualitatively evaluated by the correspondent relative variance in table 3. The majority of the grains have a grain area smaller than 20 μm^2, but a few grains have areas larger than 5 times this value – abnormal grain growth

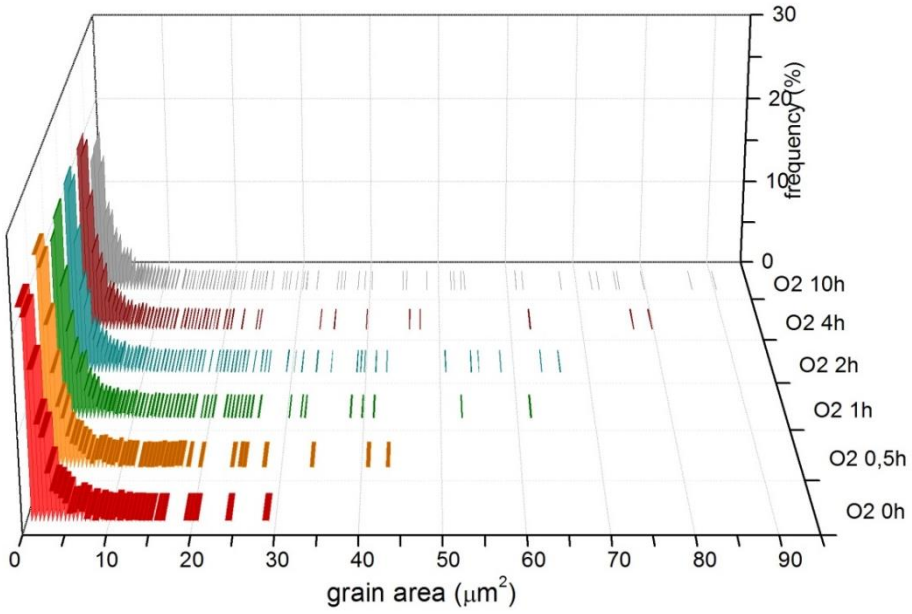

Figure 27 – Grain area distribution for samples sintered in oxygen. Larger grains present an area of 91 μm^2 for samples sintered for 10 h.

The microstructures of samples sintered in nitrogen show similar grains shape than the samples sintered in oxygen, but the grains are markedly smaller (Figure 28). In this case, the grain size distribution is more homogeneous than the grain size distribution for samples sintered in oxygen (Figure 29). Table 3 presents the relative variance that represents the values dispersion relatively to the average values. The variance increases with the increasing of the sintering time for all the sintering atmospheres. Sample sintered in oxygen for 10 h shows the higher value of variance (139), as expected, that means that this is the samples with the larger largest grains relatively to the average grain size. On the

other hand, sample sintered in nitrogen for 0 h presents the lower value of variance (~ 7) which means that this sample have a narrower grain size distribution. In addition, a relatively high amount of residual porosity is clearly visible in all of these microstructures as well as precipitates of a second phase which may correspond to the Ba_2TiO_4 phase detected in XRD.

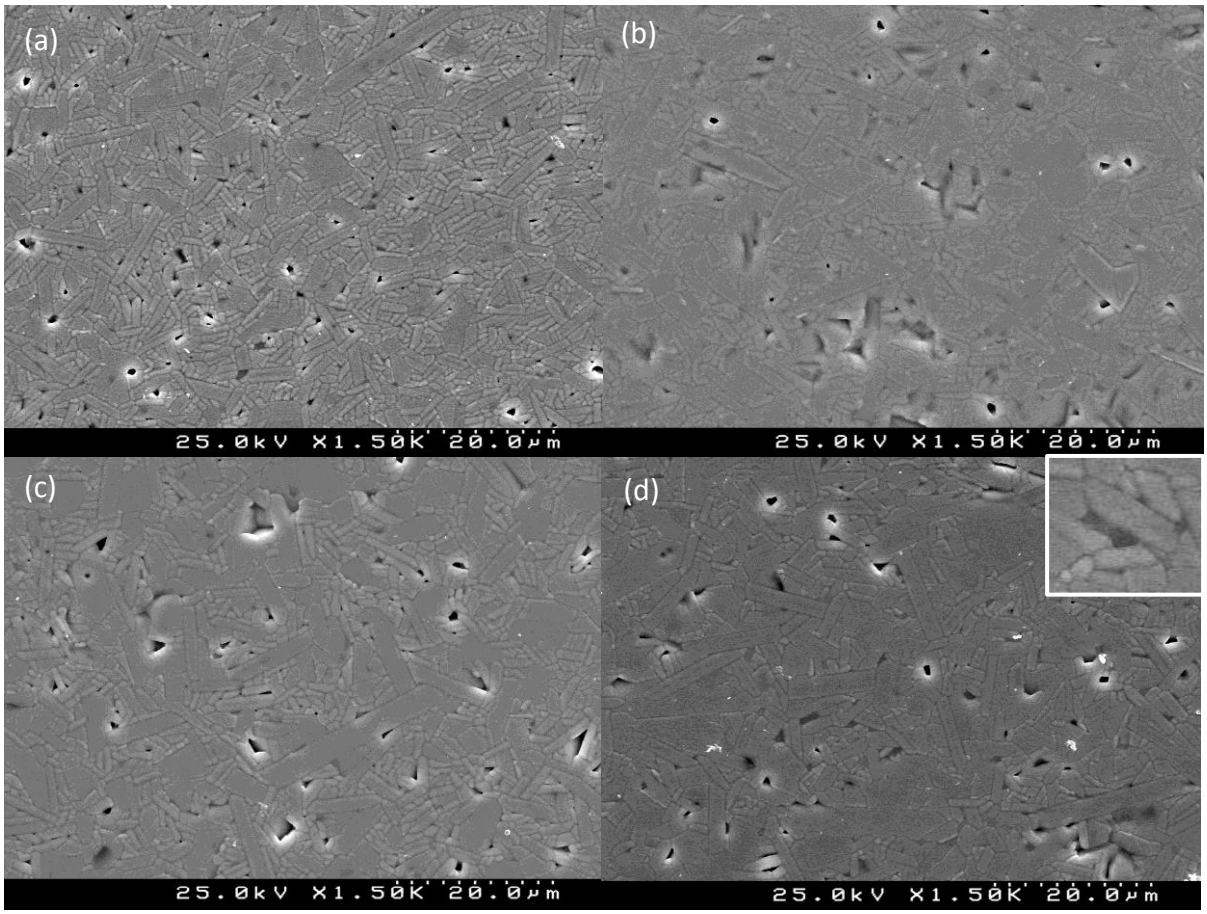

Figure 28 – SEM images of sample sintered in N_2 at (a) 0 hours, (b) 1 hour, (c) 2 hours and (d) 10 hours (inset shows the presence of a second phase). All images have the same magnification, The microstructures are characterized by elongated grains and some porosity present in the grain boundaries.

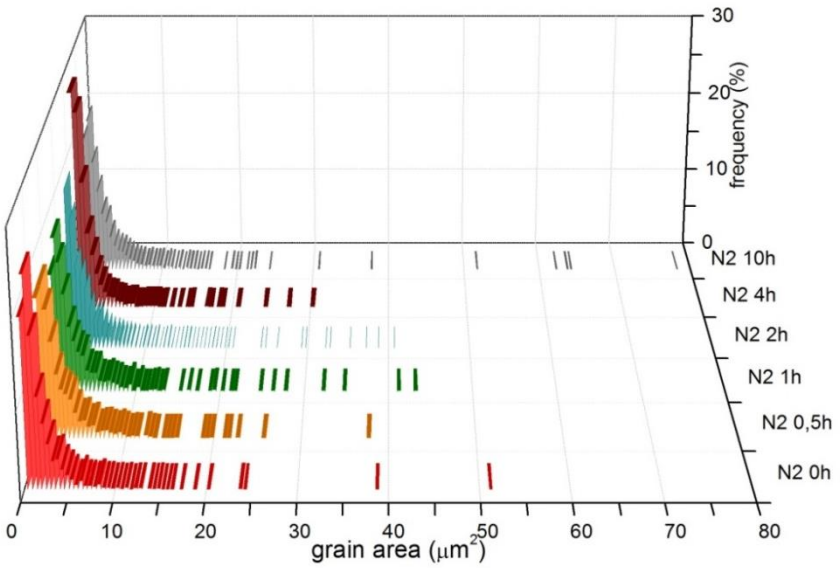

Figure 29 – Grain area distribution for samples sintered in nitrogen. The larger grains present an area of 78 μm^2 for sample sintered for 10 h.

Samples sintered in different atmospheres show different average grain areas for the same isothermal times. Samples sintered in oxygen atmospheres are continuously increasing the average grain size with time whereas for samples sintered in nitrogen it near stagnates for times longer than 2h. In Figure 31 the sintering trajectory, i.e., the average grain area in function of the relative density, are also represented for the different atmospheres; it is possible to observe that the grain size of samples sintered in nitrogen increases until ~93% of relative density and is almost constant for larger densities. For samples sintered in oxygen the grain area is smaller than that of the samples sintered in nitrogen until ~97% of relative density is attained, but for increasing values of relative density the grain area in oxygen increases and coarser microstructures can be obtained. As reported in the bibliography, stagnant effects on the grain growth of titanates can be found when stepped grain boundaries are formed [8]. These type of grain boundaries have been frequently observed in $BaTiO_3$ and $SrTiO_3$ sintered under reduced atmospheres [8].

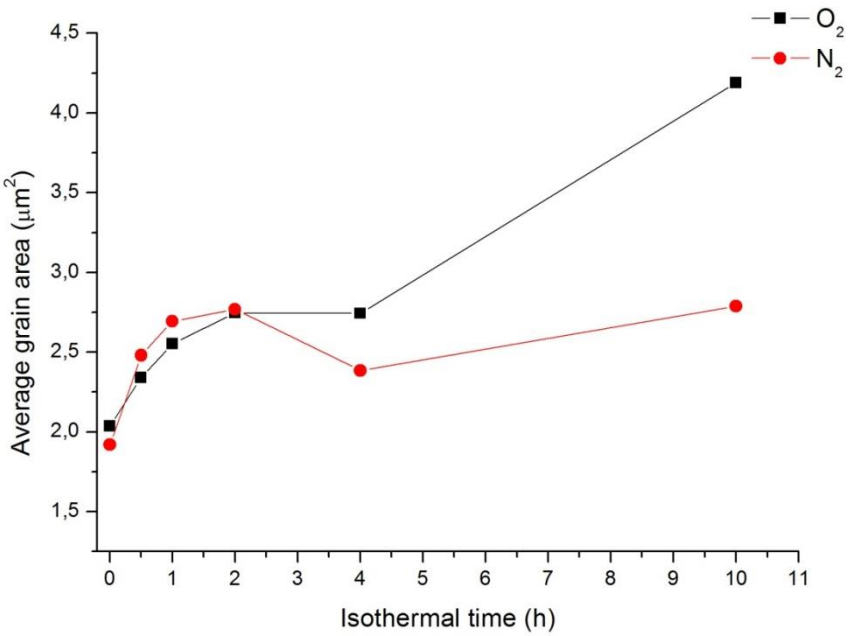

Figure 30 – Variation of the average grain area with isothermal time for different sintering atmospheres.

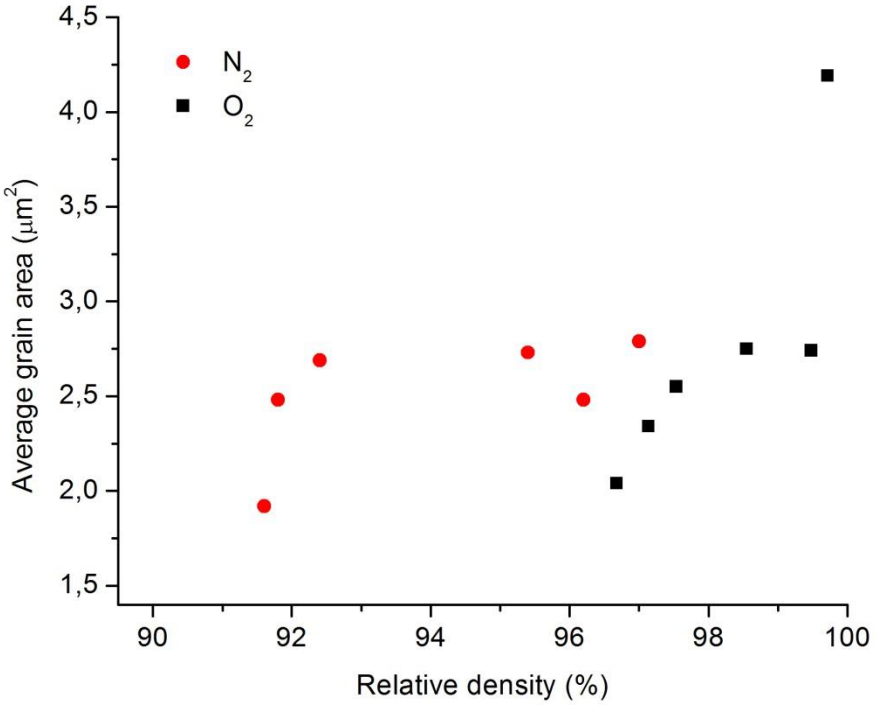

Figure 31 – Variation of average grain area with relative density for different sintering atmospheres.

The other stereological parameter analyzed was the grain aspect ratio since BLT grains are elongated and a useful characteristic is the aspect ratio that is the ratio between the grain width and height. For rounded grains the aspect ratio is equal to 1 and deviations from 1 indicate the degree of elongation.

The values of aspect ratio for the samples sintered in different atmospheres are represented in Figure 32. As the sintering time increases clearly the aspect ratio increases. A big leap occurs between 0 and 2 h of sintering and between 2 and 10 h the average aspect ratio is almost the same. The values of aspect ratio for oxygen sintered samples vary between 2.45 (0 h) and 2.9 (10 h) and for samples sintered in nitrogen aspect ratio varies between 2.42 (0h) and 2.78 (10h). As expected the oxygen atmosphere has a larger effect on the elongation of the samples than nitrogen because grains grow more (Figure 32).

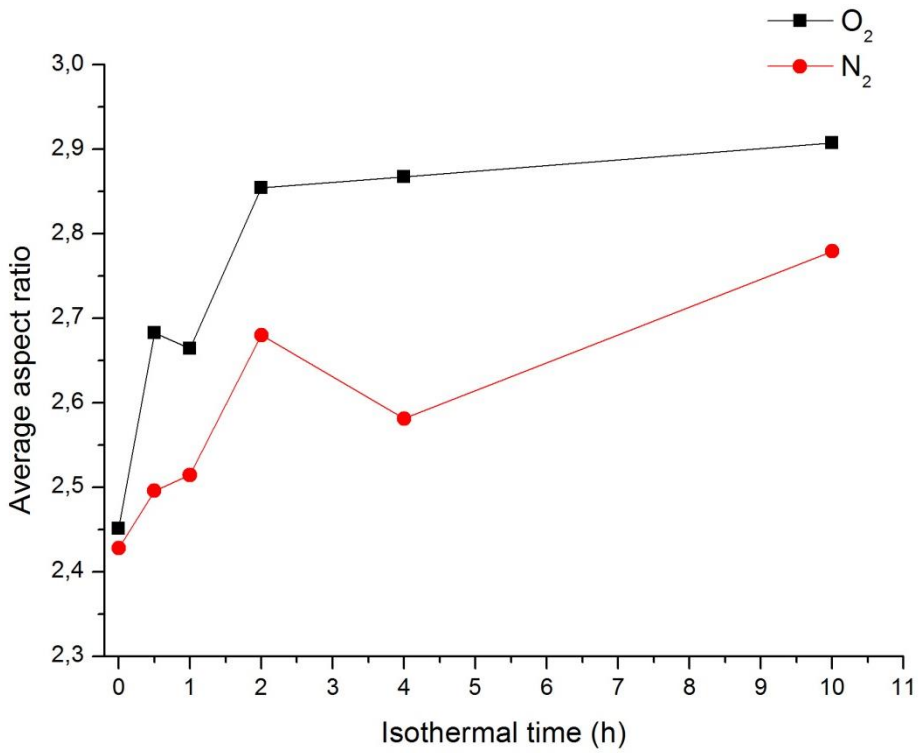

Figure 32 – Average aspect ratio in function of the isothermal time for different atmospheres. Samples sintered oxygen shows a higher aspect ratio in comparison with samples sintered in nitrogen.

For the nitrogen atmosphere the aspect ratio has a similar behaviour that grain area, for 4h of sintering. However, the sample sintered in nitrogen during 10 hours a maximum value of aspect ratio of 32 was found, which means that at least one grain have a length of 32 times the width. The sample sintered without isothermal time the maximum value of aspect ratio is 10.

The sample sintered in nitrogen for 10 hours present a maximum value of aspect ratio of 18, and 11 for samples sintered for 0 hours.

Aspect ratio maximum values show higher values in the case of oxygen than in nitrogen for the longer sintering time, which means that the increase of pO_2 in the sintering atmosphere will bring a larger anisotropy in terms of the velocity of the grain boundaries.

4.4 Electrical characterization

4.4.1 Relative permittivity and losses

The BLT samples sintered in various atmospheres with different thermal cycles were characterized by electrical measurements. The disc shaped pellets were painted with silver paste on both sides to have a metal-insulator-metal geometry and they were thermally treated by heating up to 500ºC and thoroughly checked for continuity using a multimeter. It was perceived that the influence of sintering conditions may reflect on the dielectric constant and loss tangent. The variation of relative permittivity (ε_r) with the temperature of samples sintered in oxygen and nitrogen for 0h is represented in Figure 30 and 31, for different frequencies.

It was observed that the dielectric constant of BLT samples sintered in nitrogen and oxygen atmosphere shows different trends and the values range of relative permittivity for both sintering atmospheres is different. For samples sintered in nitrogen the relative permittivity is higher than for samples sintered in oxygen. The reported dielectric constant for BLT sintered in air are ranging from 44 to 49 [37], but in our case we see that at room temperature, the value of ε_r is almost 100 for nitrogen (Figure 33 (a)) and 21.5 for oxygen

(Figure 33 (b)). This clearly shows the influence of sintering atmosphere on the electrical properties of BLT. More over at higher temperatures the behavior is different for nitrogen and oxygen, for samples sintered in nitrogen atmosphere the relative permittivity increases, reaching a value of 195, and for the samples sintered in oxygen the relative permittivity is almost constant with the increasing temperature. The difference in relative permittivity between samples sintered in nitrogen and oxygen is not possible with the presence of normal polarization. The high permittivity present in samples sintered in nitrogen could be explained with the Maxwell-Wagner polarization.

Increasing the sintering time, the relative permittivity remains higher in nitrogen than in oxygen, increasing with the temperature in both cases (Figure 34 (a) and (b)).

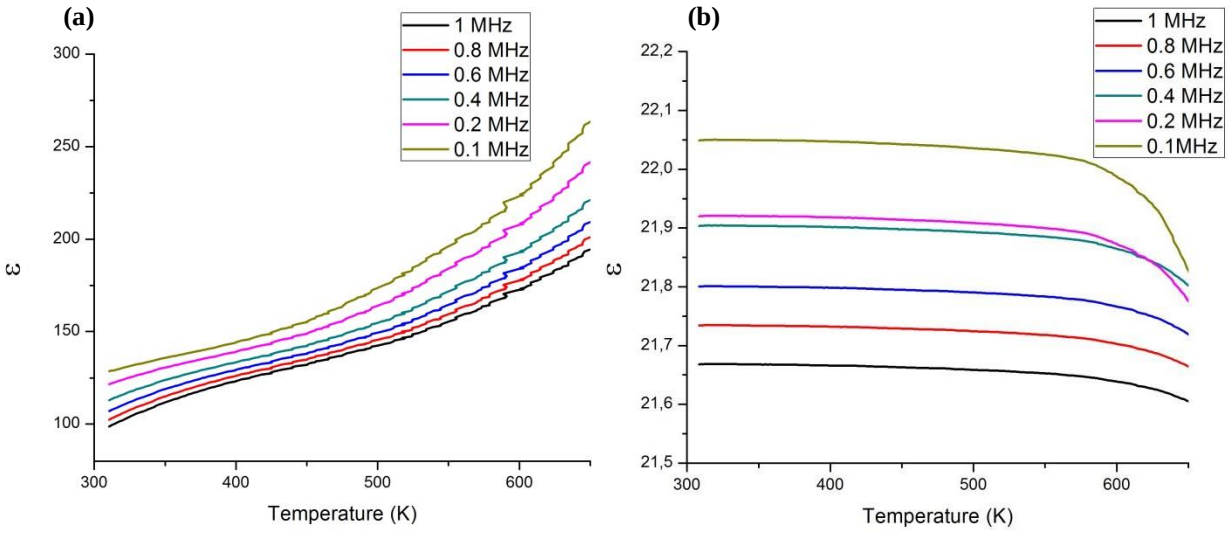

Figure 33 – Relative permittivity with temperature for samples sintered at 1530°C for 0h in (a) nitrogen and (b) oxygen. Samples sintered in nitrogen presents a higher value of relative permittivity.

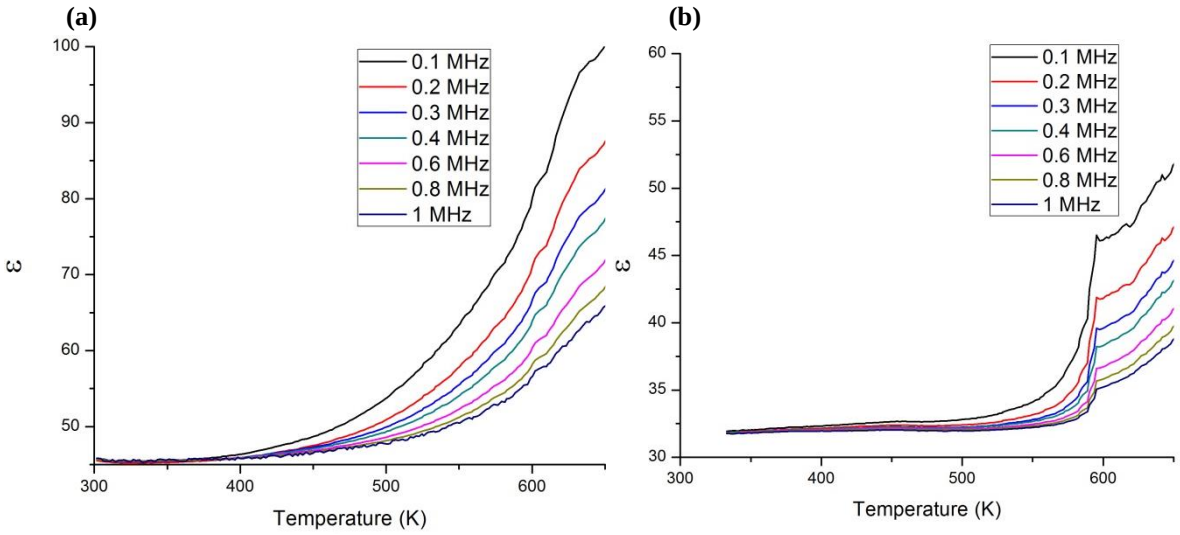

Figure 34 – Relative permittivity with temperature for samples sintered at 1530°C for 4h in (a) nitrogen and (b) oxygen. For both sintering atmospheres the relative permittivity increase with temperature, nonetheless for nitrogen the values are higher than in oxygen.

To understand the loss tangent behavior of the above mentioned samples, the dielectric losses were determined by the measurement. Figure 35 and 36 shows the variation of dielectric loss against temperature, results for the same conditions that for dielectric constant. The dielectric loss for BLT sintered in nitrogen atmosphere presents high values. Dielectric losses for samples sintered in oxygen are low but are not presented due to the sensibility of the equipment that can´t allow obtaining precise values. The presence of more defects in the nitrogen sintered samples cause a higher polarization and, consequently, a higher dielectric loss.

Samples with a higher sintering time present low dielectric losses until 400K, increasing at temperatures above this.

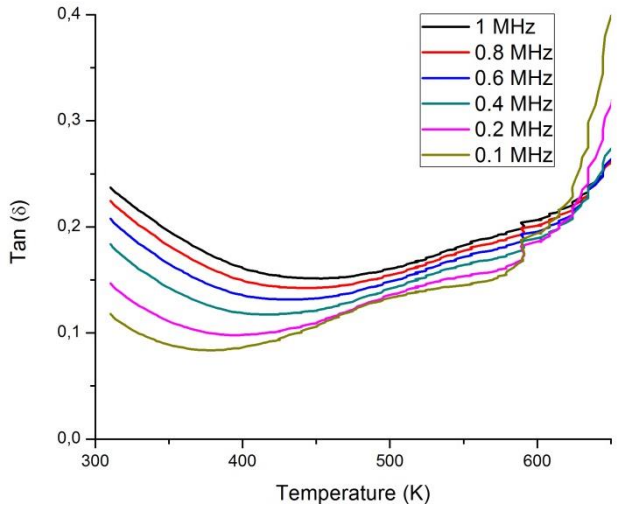

Figure 35– Dielectric losses with temperature for samples sintered at 1530°C for 0h in nitrogen. This sample shows high values of dielectric losses.

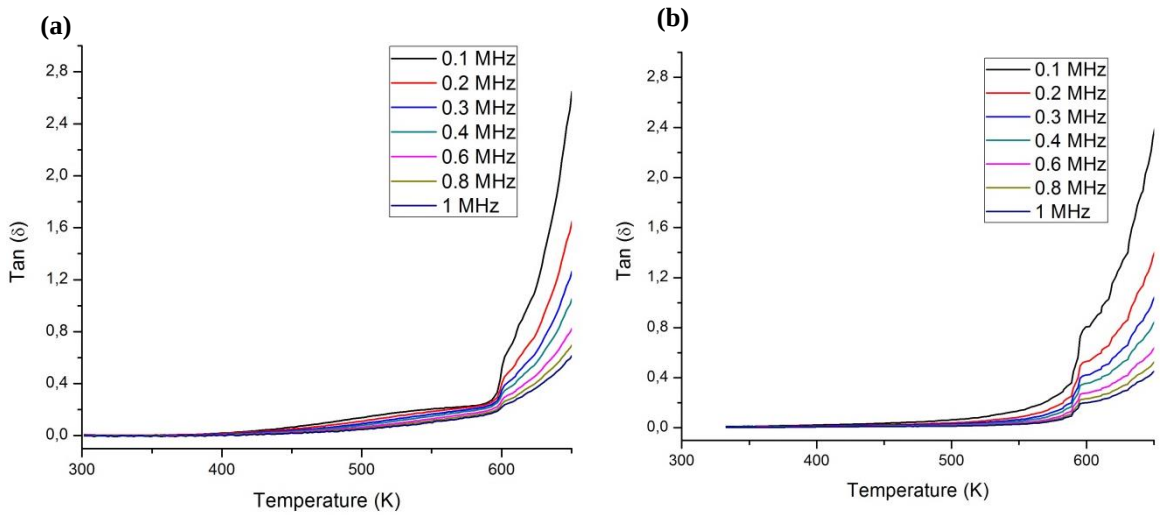

Figure 36 – Dielectric losses with temperature for samples sintered at 1530℃ for 4h in (a) nitrogen and (b) oxygen. Dielectric losses values are almost zero until temperatures until 400 K for both sintering temperatures.

The property of electrical conductivity of BLT samples was determined from the electrical measurements.

4.4.2 Conductivity

In a general way, the conductivity increases with increasing the temperature (Figure 37). Samples sintered in nitrogen for 0h presents the higher conductivity. This sample presents the lower grain size.

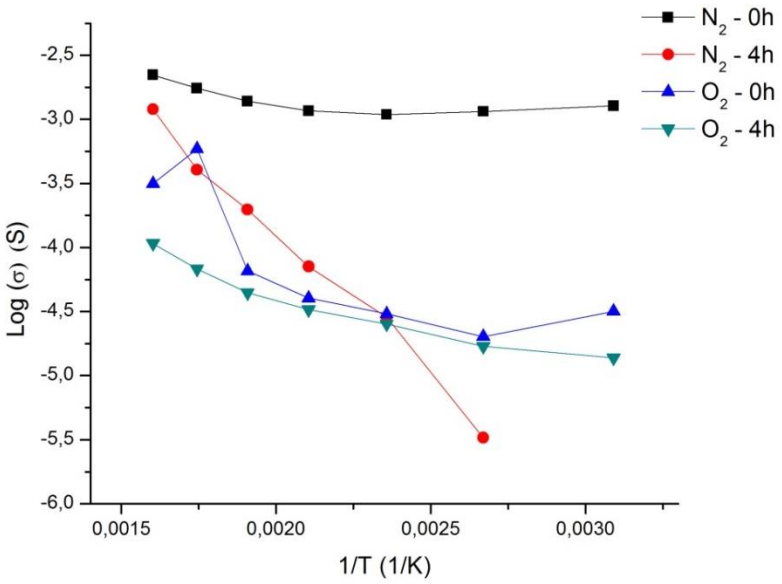

Figure 37 – Conductivity for samples sintered in nitrogen and oxygen for 0 and 4h. Samples sintered in nitrogen present a higher conductivity.

In samples sintered in nitrogen it is expected the formation of free electrons which will have a positive contribution in the conductivity. At the same time, oxygen vacancies located in the grain boundaries may create some dipoles and space charge effects, increasing the interfacial polarization and causing also higher dielectric losses.

In the case of samples sintered in oxygen, it is not expected effects of interfacial polarization and therefore lower dielectric losses values are observed.

The temperature coefficient of relative permittivity ($TC\varepsilon_r$) was obtained using the relative permittivity at room temperature and at 100ºC and the equation (2-5) was applied. Figure 37 shows the variation of $TC\varepsilon_r$ with the sintering time, for samples sintered in oxygen and nitrogen. Samples sintered more than 1 hour presents a near-zero $TC\varepsilon_r$.

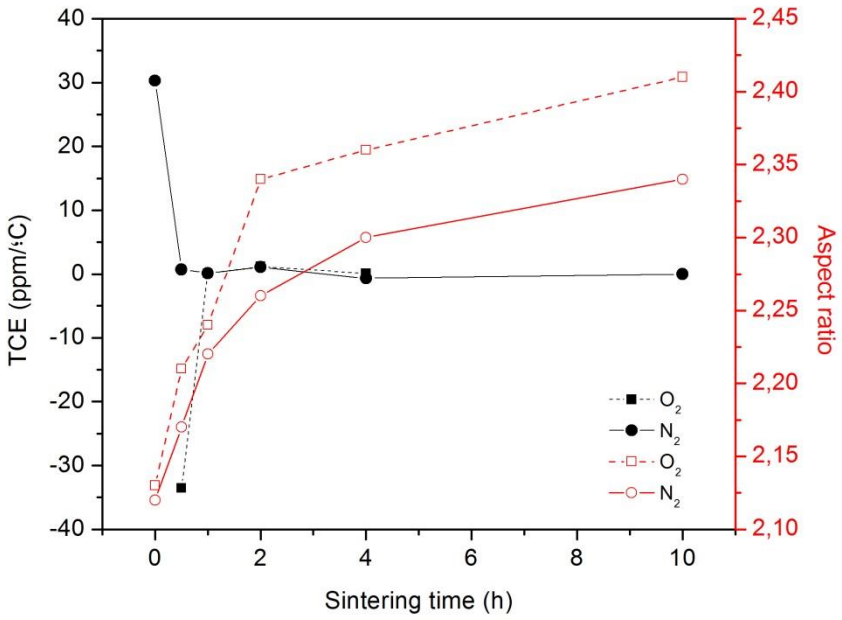

Figure 38 – Temperature coefficient of permittivity and aspect ratio with the sintering time for nitrogen and oxygen atmospheres, measured at 1 MHz.

In an oxidizing atmosphere the $TC\varepsilon_r$ and aspect ratio increases with the sintering time, but in a reducing atmosphere the opposite is observed, i.e, the aspect ratio increases and $TC\varepsilon_r$ decreases with the sintering time.

Sample sintered in nitrogen for 0 hours presents a $TC\varepsilon_r$ of 30ppm/ºC and around zero ppm/ºC for samples sintered between 30 minutes and 10 hours. Samples sintered in oxygen presents a value of $TC\varepsilon_r$ of -33ppm/ºC for a sintering time of 30 minutes and around zero for the other sintering times.

Chapter 5

Conclusions and future work

5.1 Conclusions

The effect of the atmosphere during BLT sintering was studied in this work. BLT was prepared by the conventional solid oxide mixing and a monophasic powder was obtained after calcination.

Reducing (N_2) and an oxidizing (O_2) atmosphere were used during BLT sintering, with sintering time between 0 and 10h. After sintering, all samples were analyzed by XRD and samples sintered for longer than 30 minutes, in nitrogen, and 1 hour, in oxygen, present a second phase in small quantities. A barium titanate was found in samples sintered in nitrogen due to the creation of oxygen vacancies and consequently the substitution of the barium by the lanthanum atoms. A lanthanum titanate phase was found in samples sintered in oxygen because in an oxidizing atmosphere the exsolution of lanthanum can be promoted.

The microstructure of the sintered was analyzed by SEM and the density was measured. The relative density is higher in the case of samples sintered in oxygen for all the sintering times, achieving almost the full density. Anisotropic microstructures with elongated grains were developed in the different atmospheres. Abnormal grain growth was also found to occur, namely for longer sintering times. The grain growth kinetics was found to be different in nitrogen and oxygen: in nitrogen a stagnant grain growth regimen was found after 2h of sintering, whereas in oxygen grains can grow along the sintering time. Consequently, in oxygen coarser and more anisotropic microstructures were obtained with large abnormal grains with a very high aspect ratio.

The relative permittivity was measured for samples sintered at 0 and 4 hours for both atmospheres. A higher relative permittivity was obtained for samples sintered in nitrogen for 0 hours. Samples sintered for 4h shows similar values in both atmospheres. The dielectric losses are lower and more stable with the temperature in the oxidizing atmosphere.

Conductivity increases with the temperature for all samples. The conductivity is higher for the samples sintered in nitrogen, due to the formation of free during sintering.

The values obtained in this study shows $BaLa_4Ti_4O_{15}$ is a good material for microelectronics devices miniaturization: a high dielectric permittivity is required and BLT presents an excellent value when sintered in nitrogen. However, in oxygen a low value was

achieved; low dielectric losses are needed and samples sintered in oxygen presents the lowest dielectric losses; a near-zero $TC\varepsilon_r$ is required and samples sintered in both atmospheres show a near-zero $TC\varepsilon_r$ for sintering cycles with more than 30 minutes of dwell time at 1530ºC.

5.2 Future work

Energy Dispersive Spectroscopy (EDS) is necessary in order to confirm where the second phase is in the microstructure and its composition. It is important to know the quantity of second phase present in the structure.

Transmission Electron Microscopy is essential in order to analyze the grain boundaries in detail and to go deeper on the understanding of the grain boundaries behavior in terms of mass and electrical transport.

It is important to study in detail the defect chemistry of this material since there are no studies about this topic in BLT and this is a crucial information to complete this study.

A similar study using the pressure applied during sintering as variable should be done. Literature shows that the pressure has influence on the shape of the grains and on the properties of the grain boundaries and, consequently, on the electrical properties.

Other titanates, as $BaNd_2Ti_5O_{14}$, could present interesting properties for similar applications and the influence of the sintering atmosphere should be studied.

References

(1) Rahaman, M. N. *Ceramic Processing and Sintering*; Second edi.; Marcel Dekker: New York, 2003.

(2) Amaral, L.; Jamin, C.; Senos, A. M. R.; Vilarinho, P. M.; Guillon, O. Effect of the Substrate on the Constrained Sintering of BaLa 4 Ti 4 O 15 Thick Films. *J. Am. Ceram. Soc.* **2012**, *95*, 3781–3787.

(3) Wersing, W. Microwave Ceramics for Resonators and Filters. *Curr. Opin. Solid State Mater. Sci.* **1996**, *1*, 715–731.

(4) Wilcox, N.; Ravikumar, V.; Rodrigues, R. P.; Dravid, V. P.; Vollmann, M.; Waser, R.; Soni, I. L. K.; Adriaens, A. G. Investigation of Grain Boundary Segregation in Acceptor and Donor Doped Strontium Titanate. *Solid State Ionics* **1995**, *75*.

(5) Amaral, L.; Fernandes, M.; Reaney, I. M.; Harmer, M. P.; Senos, A. M. R.; Vilarinho, P. M. Grain Growth Anomaly and Dielectric Response in Ti-Rich Strontium Titanate Ceramics. *J. Phys. Chem. C* **2013**, *117*, 24787–24795.

(6) Lee, S. B.; Lee, J.-H.; Cho, P.-S.; Kim, D.-Y.; Sigle, W.; Phillipp, F. High-Temperature Resistance Anomaly at a Strontium Titanate Grain Boundary and Its Correlation with the Grain-Boundary Faceting–Defaceting Transition. *Adv. Mater.* **2007**, *19*, 391–395.

(7) Chung, S.-Y.; Kang, S.-J. L. Effect of Sintering Atmosphere on Grain Boundary Segregation and Grain Growth in Niobium-Doped SrTiO3. *J. Am. Ceram. Soc.* **2002**, *85*, 2805–2810.

(8) Kang, S.-J. L. *Sintering: Densificaton, Grain Growth and Microstructure*; Elsevier: Great Britain, 2005.

(9) Sebastian, M. T. *Dielectric Materials for Wireless Communication*; Elsevier: Amsterdam, 2008.

(10) Cava, R. J. Dielectric Materials for Applications in Microwave Communications. *J. Mater. Chem.* **2001**, *11*, 54–62.

(11) Narang, S. B.; Bahel, S. Processing Research Low Loss Dielectric Ceramics for Microwave Applications : a Review. **2010**, *11*, 316–321.

(12) Vineis, C.; Davies, P. K.; Negas, T.; Bell, S. Microwave Dielectric Properties of Hexagonal, Perovskites. **1996**, *31*, 431–437.

(13) Teneze, N.; Mercurio, D.; Trolliard, G.; Frit, B. Cation-Deficient Perovskite-Related Compounds from Neutron Powder Diffraction Data. **2000**, *35*, 1603–1614.

(14) Moulson, A. J.; Herbert, J. M. *Electroceramics: Materials, Properties, Applications*; Second edi.; John Wiley & Sons: Great Britain, 2003.

(15) Harre, N.; Mercurio, D.; Trolliard, G.; Frit, B. Crystal Structure of BaLa4Ti4O15, Member N=5 of the Homologous Series (Ba,La)nTin-1O3n of Cation-Deficient Perovskite-Related Compounds. *Mater. Res. Bull.* **1998**, *33*, 1537–1548.

(16) Amaral, L. Design of Titanate-Based Electroceramics, Universidade de Aveiro, 2012.

(17) Reaney, I. M.; Colla, E. L.; Setter, N. No Title. *Jpn. J. Appl. Phys.* **1994**, *33*, 3984–3990.

(18) Fu, Z.; Vilarinho, P. M.; Wu, A.; Kingon, A. I. Textured Microstructure and Dielectric Properties Relationship of BaNd 2 Ti 5 O 14 Thick Films Prepared by Electrophoretic Deposition. *Adv. Funct. Mater.* **2009**, *19*, 1071–1081.

(19) Zheng, H.; Woodward, D. I.; Gillie, L.; Reaney, I. M. Structure and Microwave Dielectric Properties of BaLa4Ti4O15. *J. Phys. Condens. Matter* **2006**, *18*, 7051–7062.

(20) Okawa, T.; Kiuchi, K.; Okabe, H. Ferroelectrics Microwave Dielectric Properties of Ba n La 4 Ti 3 + n O 12 + 3 n Homologous Compounds and Substitution of Trivalent Cations for La. *Ferroelectrics* **2002**, *272*, 345–350.

(21) Jawahar, I. N.; Santha, N. I.; Thomas, M. Microwave Dielectric Properties of MO – La 2 O 3 – TiO 2 (M = Ca , Sr , Ba) Ceramics. *J. Mater. Res.* **2002**, *2*, 3084–3089.

(22) J.W. Morris, J. No Title. In *Materials Science and engineering*; Berkeley; pp. 76–107.

(23) Fukami, Y.; Wada, K.; Kakimoto, K.; Ohsato, H. Microstructure and Microwave Dielectric Properties of BaLa4Ti4O15 Ceramics with Template Particles. *J. Eur. Ceram. Soc.* **2006**, *26*, 2055–2058.

(24) Rohrer, G. S. Grain Boundary Energy Anisotropy: a Review. *J. Mater. Sci.* **2011**, *46*, 5881–5895.

(25) Yan, L. C.; Hassan, J.; Hashim, M.; Yin, W. S.; Khoon, T. F.; Jeng, W. Y. Effect of Sintering Temperatures on the Microstructure and Dielectric Properties of SrTiO 3. *World Appl. Sci. J.* **2011**, *14*, 1091–1094.

(26) Schmidt, R.; Stennett, M. C.; Hyatt, N. C.; Pokorny, J.; Prado-gonjal, J.; Li, M.; Sinclair, D. C. Effects of Sintering Temperature on the Internal Barrier Layer Capacitor (IBLC) Structure in CaCu3Ti4O12 (CCTO) Ceramics. *J. Eur. Ceram. Soc.* **2012**, *32*, 3313–3323.

(27) Chao, S.; Petrovsky, V.; Dogan, F. Effects of Sintering Temperature on the Microstructure and Dielectric Properties of Titanium Dioxide Ceramics. *J. Mater. Sci.* **2010**, *45*, 6685–6693.

(28) Park, M.; Cho, N. The Effect of the Sintering Atmosphere on the Electrical and Chemical Characteristics of Grain Boundaries in SrTiO 3 Ceramics Prepared from Semiconducting Powders. *Solid State Ionics* **2002**, *155*, 175–181.

(29) Fujimoto, M.; Chiang, Y.-M.; Roshko, A.; Kingery, W. D. Microstructure and Electrical Properties of Sodium-Diffused and Potassium-Diffused SrTiO3 Barrier-Layer Capacitors Exhibiting Varistor Behavior. *J. Am. Ceram. Soc.* **2006**, *68*, 300–303.

(30) Li, J.; Li, S.; Alim, M. a. The Effect of Reducing Atmosphere on the SrTiO3 Based Varistor-Capacitor Materials. *J. Mater. Sci. Mater. Electron.* **2006**, *17*, 503–508.

(31) Jung, Y.; Choi, S.; Kang, S. Effect of Oxygen Partial Pressure on Grain Boundary Structure and Grain Growth Behavior in BaTiO3. *Acta Mater.* **2006**, *54*, 2849–2855.

(32) Kim, B. K.; Lee, H. S.; Lee, J. W.; Lee, S. E.; Cho, Y. S. Dielectric and Grain-Boundary Characteristics of Hot Pressed CaCu3Ti4O12. *J. Am. Ceram. Soc.* **2010**, *93*, 2419–2422.

(33) Besson, J.; Abouaf, M. Microstructural Changes in Alumina During Hot Isostatic Pressing. *Mater. Sci. Eng. A* **1989**, *109*, 37–43.

(34) Besson, J.; Abouaf, M. Grain Growth Enhancement in Alumina During Hot Isostatic Pressing. *Acta Metall. Mater.* **1991**, *39*, 2225–2234.

(35) Pratten, N. A. Review The Precise Measurement of the Density of Small Samples. *J. Mater. Sci.* **1981**, *16*, 1737–1747.

(36) ImageJ http://rsb.info.nih.gov/ij (accessed Jan 15, 2013).

(37) Mahajan, A. Fabrication of Composite Thick Films of BaLa4Ti4O15 and Ba4Nd9.33Ti18O54 by Electrophoretic Deposition, Universidade de Aveiro, 2009.

(38) Fu, Z. BaNd2Ti5O14 Thick Films for Microelectronics Fabricated by Electrophoretic Deposition, University of Aveiro, 2008.